

Life Cycle Cost Analysis in Resilient Structural System Development

Lead Guest Editor: Juan Bojórquez

Guest Editors: Sonia E. Ruiz, Edén Bojórquez, Alfredo Reyes-Salazar, and Antonio Formisano





Life Cycle Cost Analysis in Resilient Structural System Development

Advances in Civil Engineering

Life Cycle Cost Analysis in Resilient Structural System Development

Lead Guest Editor: Juan Bojórquez

Guest Editors: Sonia E. Ruiz, Edén Bojórquez,
Alfredo Reyes-Salazar, and Antonio Formisano



Copyright © 2022 Hindawi Limited. All rights reserved.

This is a special issue published in "Advances in Civil Engineering." All articles are open access articles distributed under the Creative Commons Attribution License, which permits unrestricted use, distribution, and reproduction in any medium, provided the original work is properly cited.


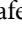
Chief Editor

Cumaraswamy Vipulanandan, USA










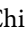



Associate Editors

Chiara Bedon , Italy
Constantin Chalioris , Greece
Ghassan Chehab , Lebanon
Ottavia Corbi, Italy
Mohamed ElGawady , USA
Husnain Haider , Saudi Arabia
Jian Ji , China
Jiang Jin , China
Shazim A. Memon , Kazakhstan
Hossein Moayedi , Vietnam
Sanjay Nimbalkar, Australia
Giuseppe Oliveto , Italy
Alessandro Palmeri , United Kingdom
Arnaud Perrot , France
Hugo Rodrigues , Portugal
Victor Yepes , Spain
Xianbo Zhao , Australia

Academic Editors

José A.F.O. Correia, Portugal
Glenda Abate, Italy
Khalid Abdel-Rahman , Germany
Ali Mardani Aghabaglou, Turkey
José Aguiar , Portugal
Afaq Ahmad , Pakistan
Muhammad Riaz Ahmad , Hong Kong
Hashim M.N. Al-Madani , Bahrain
Luigi Aldieri , Italy
Angelo Aloisio , Italy
Maria Cruz Alonso, Spain
Filipe Amarante dos Santos , Portugal
Serji N. Amirkhanean, USA
Eleftherios K. Anastasiou , Greece
Panagiotis Ch. Anastasopoulos , USA
Mohamed Moafak Arbili , Iraq
Farhad Aslani , Australia
Siva Avudaiappan , Chile
Ozgur BASKAN , Turkey
Adewumi Babafemi, Nigeria
Morteza Bagherpour, Turkey
Qingsheng Bai , Germany
Nicola Baldo , Italy
Daniele Baraldi , Italy

Eva Barreira , Portugal
Emilio Bastidas-Arteaga , France
Rita Bento, Portugal
Rafael Bergillos , Spain
Han-bing Bian , China
Xia Bian , China
Huseyin Bilgin , Albania
Giovanni Biondi , Italy
Hugo C. Biscaia , Portugal
Rahul Biswas , India
Edén Bojórquez , Mexico
Giosuè Boscato , Italy
Melina Bosco , Italy
Jorge Branco , Portugal
Bruno Briseghella , China
Brian M. Broderick, Ireland
Emanuele Brunesi , Italy
Quoc-Bao Bui , Vietnam
Tan-Trung Bui , France
Nicola Buratti, Italy
Gaochuang Cai, France
Gladis Camarini , Brazil
Alberto Campisano , Italy
Qi Cao, China
Qixin Cao, China
Iacopo Carnacina , Italy
Alessio Cascardi, Italy
Paolo Castaldo , Italy
Nicola Cavalagli , Italy
Liborio Cavaleri , Italy
Anush Chandrappa , United Kingdom
Wen-Shao Chang , United Kingdom
Muhammad Tariq Amin Chaudhary, Kuwait
Po-Han Chen , Taiwan
Qian Chen , China
Wei Tong Chen , Taiwan
Qixiu Cheng, Hong Kong
Zhanbo Cheng, United Kingdom
Nicholas Chileshe, Australia
Prinya Chindaprasirt , Thailand
Corrado Chisari , United Kingdom
Se Jin Choi , Republic of Korea
Heap-Yih Chong , Australia
S.H. Chu , USA
Ting-Xiang Chu , China

Zhaofei Chu , China
Wonseok Chung , Republic of Korea
Donato Ciampa , Italy
Gian Paolo Cimellaro, Italy
Francesco Colangelo, Italy
Romulus Costache , Romania
Liviu-Adrian Cotfas , Romania
Antonio Maria D'Altri, Italy
Bruno Dal Lago , Italy
Amos Darko , Hong Kong
Arka Jyoti Das , India
Dario De Domenico , Italy
Gianmarco De Felice , Italy
Stefano De Miranda , Italy
Maria T. De Risi , Italy
Tayfun Dede, Turkey
Sadik O. Degertekin , Turkey
Camelia Delcea , Romania
Cristoforo Demartino, China
Giuseppe Di Filippo , Italy
Luigi Di Sarno, Italy
Fabio Di Trapani , Italy
Aboelkasim Diab , Egypt
Thi My Dung Do, Vietnam
Giulio Dondi , Italy
Jiangfeng Dong , China
Chao Dou , China
Mario D'Aniello , Italy
Jingtao Du , China
Ahmed Elghazouli, United Kingdom
Francesco Fabbrocino , Italy
Flora Faleschini , Italy
Dingqiang Fan, Hong Kong
Xueping Fan, China
Qian Fang , China
Salar Farahmand-Tabar , Iran
Ilenia Farina, Italy
Roberto Fedele, Italy
Guang-Liang Feng , China
Luigi Fenu , Italy
Tiago Ferreira , Portugal
Marco Filippo Ferrotto, Italy
Antonio Formisano , Italy
Guoyang Fu, Australia
Stefano Galassi , Italy

Junfeng Gao , China
Meng Gao , China
Giovanni Garcea , Italy
Enrique García-Macías, Spain
Emilio García-Taengua , United Kingdom
DongDong Ge , USA
Khaled Ghaedi, Malaysia
Khaled Ghaedi , Malaysia
Gian Felice Giaccu, Italy
Agathoklis Giaralis , United Kingdom
Ravindran Gobinath, India
Rodrigo Gonçalves, Portugal
Peilin Gong , China
Belén González-Fonteboa , Spain
Salvatore Grasso , Italy
Fan Gu, USA
Erhan Güneyisi , Turkey
Esra Mete Güneyisi, Turkey
Pingye Guo , China
Ankit Gupta , India
Federico Gusella , Italy
Kemal Hacıefendioğlu, Turkey
Jianyong Han , China
Song Han , China
Asad Hanif , Macau
Hadi Hasanzadehshooiili , Canada
Mostafa Fahmi Hassanein, Egypt
Amir Ahmad Hedayat , Iran
Khandaker Hossain , Canada
Zahid Hossain , USA
Chao Hou, China
Biao Hu, China
Jiang Hu , China
Xiaodong Hu, China
Lei Huang , China
Cun Hui , China
Bon-Gang Hwang, Singapore
Jijo James , India
Abbas Fadhil Jasim , Iraq
Ahad Javanmardi , China
Krishnan Prabhakan Jaya, India
Dong-Sheng Jeng , Australia
Han-Yong Jeon, Republic of Korea
Pengjiao Jia, China
Shaohua Jiang , China

MOUSTAFA KASSEM , Malaysia
Mosbeh Kaloop , Egypt
Shankar Karuppannan , Ethiopia
John Kechagias , Greece
Mohammad Khajehzadeh , Iran
Afzal Husain Khan , Saudi Arabia
Mehran Khan , Hong Kong
Manoj Khandelwal, Australia
Jin Kook Kim , Republic of Korea
Woosuk Kim , Republic of Korea
Vaclav Koci , Czech Republic
Loke Kok Foong, Vietnam
Hailing Kong , China
Leonidas Alexandros Kouris , Greece
Kyriakos Kourousis , Ireland
Moacir Kripka , Brazil
Anupam Kumar, The Netherlands
Emma La Malfa Ribolla, Czech Republic
Ali Lakirouhani , Iran
Angus C. C. Lam, China
Thanh Quang Khai Lam , Vietnam
Luciano Lamberti, Italy
Andreas Lampropoulos , United Kingdom
Raffaele Landolfo, Italy
Massimo Latour , Italy
Bang Yeon Lee , Republic of Korea
Eul-Bum Lee , Republic of Korea
Zhen Lei , Canada
Leonardo Leonetti , Italy
Chun-Qing Li , Australia
Dongsheng Li , China
Gen Li, China
Jiale Li , China
Minghui Li, China
Qingchao Li , China
Shuang Yang Li , China
Sunwei Li , Hong Kong
Yajun Li , China
Shun Liang , China
Francesco Liguori , Italy
Jae-Han Lim , Republic of Korea
Jia-Rui Lin , China
Kun Lin , China
Shibin Lin, China

Tzu-Kang Lin , Taiwan
Yu-Cheng Lin , Taiwan
Hexu Liu, USA
Jian Lin Liu , China
Xiaoli Liu , China
Xuemei Liu , Australia
Zaobao Liu , China
Zhuang-Zhuang Liu, China
Diego Lopez-Garcia , Chile
Cristiano Loss , Canada
Lyan-Ywan Lu , Taiwan
Jin Luo , USA
Yanbin Luo , China
Jianjun Ma , China
Junwei Ma , China
Tian-Shou Ma, China
Zhongguo John Ma , USA
Maria Macchiaroli, Italy
Domenico Magisano, Italy
Reza Mahinroosta, Australia
Yann Malecot , France
Prabhat Kumar Mandal , India
John Mander, USA
Iman Mansouri, Iran
André Dias Martins, Portugal
Domagoj Matesan , Croatia
Jose Matos, Portugal
Vasant Matsagar , India
Claudio Mazzotti , Italy
Ahmed Mebarki , France
Gang Mei , China
Kasim Mermerdas, Turkey
Giovanni Minafò , Italy
Masoomah Mirrashid , Iran
Abbas Mohajerani , Australia
Fadzli Mohamed Nazri , Malaysia
Fabrizio Mollaioli , Italy
Rosario Montuori , Italy
H. Naderpour , Iran
Hassan Nasir , Pakistan
Hossein Nassiraei , Iran
Satheeskumar Navaratnam , Australia
Ignacio J. Navarro , Spain
Ashish Kumar Nayak , India
Behzad Nematollahi , Australia

Chayut Ngamkhanong , Thailand
Trung Ngo, Australia
Tengfei Nian, China
Mehdi Nikoo , Canada
Youjun Ning , China
Olugbenga Timo Oladinrin , United Kingdom
Oladimeji Benedict Olalusi, South Africa
Timothy O. Olawumi , Hong Kong
Alejandro Orfila , Spain
Maurizio Orlando , Italy
Siti Aminah Osman, Malaysia
Walid Oueslati , Tunisia
SUVASH PAUL , Bangladesh
John-Paris Pantouvakis , Greece
Fabrizio Paolacci , Italy
Giuseppina Pappalardo , Italy
Fulvio Parisi , Italy
Dimitrios G. Pavlou , Norway
Daniele Pellegrini , Italy
Gatheeshgar Perampalam , United Kingdom
Daniele Perrone , Italy
Giuseppe Piccardo , Italy
Vagelis Plevris , Qatar
Andrea Pranno , Italy
Adolfo Preciado , Mexico
Chongchong Qi , China
Yu Qian, USA
Ying Qin , China
Giuseppe Quaranta , Italy
Krishanu ROY , New Zealand
Vlastimir Radonjanin, Serbia
Carlo Rainieri , Italy
Rahul V. Ralegaonkar, India
Raizal Saifulnaz Muhammad Rashid, Malaysia
Alessandro Rasulo , Italy
Chonghong Ren , China
Qing-Xin Ren, China
Dimitris Rizos , USA
Geoffrey W. Rodgers , New Zealand
Pier Paolo Rossi, Italy
Nicola Ruggieri , Italy
JUNLONG SHANG, Singapore






Nikhil Saboo, India
Anna Saetta, Italy
Juan Sagaseta , United Kingdom
Timo Saksala, Finland
Mostafa Salari, Canada
Ginevra Salerno , Italy
Evangelos J. Sapountzakis , Greece
Vassilis Sarhosis , United Kingdom
Navaratnarajah Sathiparan , Sri Lanka
Fabrizio Scozzese , Italy
Halil Sezen , USA
Payam Shafigh , Malaysia
M. Shahria Alam, Canada
Yi Shan, China
Hussein Sharaf, Iraq
Mostafa Sharifzadeh, Australia
Sanjay Kumar Shukla, Australia
Amir Si Larbi , France
Okan Sirin , Qatar
Piotr Smarzewski , Poland
Francesca Sollecito , Italy
Rui Song , China
Tian-Yi Song, Australia
Flavio Stochino , Italy
Mayank Sukhija , USA
Piti Sukontasukkul , Thailand
Jianping Sun, Singapore
Xiao Sun , China
T. Tafsirojjan , Australia
Fujiao Tang , China
Patrick W.C. Tang , Australia
Zhi Cheng Tang , China
Weerachart Tangchirapat , Thailand
Xiabin Tao, China
Piergiorgio Tataranni , Italy
Elisabete Teixeira , Portugal
Jorge Iván Tobón , Colombia
Jing-Zhong Tong, China
Francesco Trentadue , Italy
Antonello Troncone, Italy
Majbah Uddin , USA
Tariq Umar , United Kingdom
Muahmmad Usman, United Kingdom
Muhammad Usman , Pakistan
Mucteba Uysal , Turkey

Ilaria Venanzi , Italy
Castorina S. Vieira , Portugal
Valeria Vignali , Italy
Claudia Vitone , Italy
Liwei WEN , China
Chunfeng Wan , China
Hua-Ping Wan, China
Roman Wan-Wendner , Austria
Chaohui Wang , China
Hao Wang , USA
Shiming Wang , China
Wayne Yu Wang , United Kingdom
Wen-Da Wang, China
Xing Wang , China
Xiuling Wang , China
Zhenjun Wang , China
Xin-Jiang Wei , China
Tao Wen , China
Weiping Wen , China
Lei Weng , China
Chao Wu , United Kingdom
Jiangyu Wu, China
Wangjie Wu , China
Wenbing Wu , China
Zhixing Xiao, China
Gang Xu, China
Jian Xu , China
Panpan , China
Rongchao Xu , China
HE YONGLIANG, China
Michael Yam, Hong Kong
Hailu Yang , China
Xu-Xu Yang , China
Hui Yao , China
Xinyu Ye , China
Zhoujing Ye, China
Gürol Yildirim , Turkey
Dawei Yin , China
Doo-Yeol Yoo , Republic of Korea
Zhanping You , USA
Afshar A. Yousefi , Iran
Xinbao Yu , USA
Dongdong Yuan , China
Geun Y. Yun , Republic of Korea




Hyun-Do Yun , Republic of Korea
Cemal YİĞİT , Turkey
Paolo Zampieri, Italy
Giulio Zani , Italy
Mariano Angelo Zanini , Italy
Zhixiong Zeng , Hong Kong
Mustafa Zeybek, Turkey
Henglong Zhang , China
Jiupeng Zhang, China
Tingting Zhang , China
Zengping Zhang, China
Zetian Zhang , China
Zhigang Zhang , China
Zhipeng Zhao , Japan
Jun Zhao , China
Annan Zhou , Australia
Jia-wen Zhou , China
Hai-Tao Zhu , China
Peng Zhu , China
QuanJie Zhu , China
Wenjun Zhu , China
Marco Zucca, Italy
Haoran Zuo, Australia
Junqing Zuo , China
Robert Černý , Czech Republic
Süleyman İpek , Turkey

Contents

Development an Artificial Neural Network Model for Estimating Cost of R/C Building by Using Life-Cycle Cost Function: Case Study of Mexico City

Henry E. Reyes, Juan Bojórquez , Laura Cruz-Reyes, Sonia E. Ruiz , Alfredo Reyes-Salazar, Edén Bojórquez , Manuel Barraza , Antonio Formisano, Omar Payán , and José R. Torres
Research Article (15 pages), Article ID 7418230, Volume 2022 (2022)

Neural Network Based Estimation of Service Life of Different Metal Culverts in Arkansas

Zahid Hossain , MdAriful Hasan , and Rouzbeh Ghabchi 
Research Article (10 pages), Article ID 6860287, Volume 2022 (2022)

Research Article

Development an Artificial Neural Network Model for Estimating Cost of R/C Building by Using Life-Cycle Cost Function: Case Study of Mexico City

Henry E. Reyes,¹ Juan Bojórquez ,¹ Laura Cruz-Reyes,² Sonia E. Ruiz ,³ Alfredo Reyes-Salazar,¹ Edén Bojórquez ,¹ Manuel Barraza ,⁴ Antonio Formisano,⁵ Omar Payán ,⁶ and José R. Torres⁶

¹Facultad de Ingeniería, Universidad Autónoma de Sinaloa, Culiacán 80013, Mexico

²Instituto Tecnológico de Ciudad Madero, Ciudad Madero, Tamaulipas, Mexico

³Instituto de Ingeniería, Universidad Nacional Autónoma de México, Coyoacán 04510, Mexico

⁴Facultad de Ingeniería, Arquitectura y Diseño, Universidad Autónoma de Baja California, Ensenada 22860, Mexico

⁵Department of Structures for Engineering and Architecture, University of Naples, Naples 80125, Italy

⁶Department of Mechanical and Mechatronic Engineering, Tecnológico Nacional de México, Culiacán, Sinaloa, Mexico

Correspondence should be addressed to Juan Bojórquez; juanbm@uas.edu.mx, Edén Bojórquez; eden@uas.edu.mx, Manuel Barraza; barraza.manuel@uabc.edu.mx, and Omar Payán; omarjps@hotmail.com

Received 27 January 2022; Revised 10 March 2022; Accepted 13 March 2022; Published 12 April 2022

Academic Editor: Qian Chen

Copyright © 2022 Henry E. Reyes et al. This is an open access article distributed under the Creative Commons Attribution License, which permits unrestricted use, distribution, and reproduction in any medium, provided the original work is properly cited.

This paper addresses the importance of engineering asset management decisions and control. For this purpose, a Life-Cycle Cost (LCC) analysis is conducted for typical reinforced concrete (R/C) buildings located in Mexico City. The objective of this study is to develop an artificial neural network (ANN) model that can estimate the total expected cost of R/C buildings by using LCC functions. The total cost includes the initial cost and the cost of the damage caused by future possible ground motions at the site of interest. The present value of the cost includes: initial cost, repair or reconstruction cost, cost of damage to the contents, costs associated with the loss of life or injuries and economic losses. The structural performance is evaluated using probabilistic models, artificial neural networks models are used to obtain the seismic response of the buildings. The methodology is applied to a set of reinforced concrete buildings with 4, 8, and 12 stories which are located at the soft soil of Mexico City. Finally, it is concluded that the life-cycle cost is efficiently obtained using artificial neural network models for estimating the structural reliability of reinforced concrete buildings, in such a way that it can be used as an excellent planning tool that covers long spans of time.

1. Introduction

The life-cycle cost estimation has received abundant attention over the past decades. In that time, the challenge of estimating the total life-cycle costs of structures considering all variables involved in the problem has represented a difficult task. There is a vast amount of literature available regarding the estimation of the expected cost for different structural systems [1–19]; however, those studies generally are applied to a limited number of particular cases. Furthermore, one of the main limitations of those studies is the

time consuming of the methodology to obtain the total expected cost. This study addresses this issue, to perform this task artificial neural networks are used aiming to minimize the time consuming of the methodology within low errors in the estimation. The great potential of ANNs is the high-speed processing provided in a massive parallel implementation [20]. ANNs can be developed and used for image recognition, natural language processing and so on. Nowadays, ANNs are vastly used for universal function approximation in numerical paradigms because of their excellent properties of self-learning, adaptivity, fault

tolerance, nonlinearity, and advancement in input and output mapping [21]. In the engineering field ANN has been used for optimization and seismic code calibration [22], they have been applied for estimating concrete and reinforcement consumption in the construction of integral bridges [23]; moreover, an artificial neural network model has been applied to estimate the construction costs [24]. For bridge design an ANN was used to decrease the computational demand of box-girder element analysis [25]. The prediction and identification of seismic-induced damage in structures has been possible using neural networks [26–28]. For earthquake engineering, the use of the power of ANN pattern recognition was applied to evaluate seismic risk problems [29].

The estimation of the life-cycle cost of buildings is a primary part of a construction project, it is considered one of the major criteria in building design for its importance in helping to choose economic structural configurations and to estimate future costs of ownership. In this paper, it is considered that the total expected life-cycle cost of buildings includes: the initial costs plus the expected costs of the damage caused to the structure by future earthquakes, including repair cost, cost of damage to the contents, the cost associated with the loss of life and injuries, and direct economic losses [30]. The loads considered for the structural design are: dead load, life load, and earthquake loads. The structural performance is evaluated using probabilistic analysis. The occurrence of earthquakes is described by a Poisson process [31]. The methodology is applied to a set of reinforced concrete buildings with 4, 8, and 12 stories (low, middle and high rise) located in soft soil with ground period of $T_s = 2.0s$ of Mexico City, which are of main concern in Mexico City Building Code (MCBC). Finally, it is concluded that artificial intelligence can provide accurate results, minimize prediction errors, and it can be used as an excellent planning tool that covers long spans of time.

2. General Methodology

The general approach taken to obtain the life-cycle costs of buildings is summarized in the steps below and illustrated in Figure 1.

2.1. Structural Design of Buildings (Step 1). The buildings are designed according to the Mexico City Building Code considering the seismic design and concrete regulations for buildings located in the soft soil of Mexico City.

2.2. Maximum Structural Capacity (Step 2). The maximum structural capacity is obtained using incremental dynamic analysis (IDA) [32]. For this aim, the maximum inter-story drift (MID) is selected as the engineering demand parameter to conduct the analysis. The associated yielding and near collapse limit states of the buildings can be obtained from this analysis.

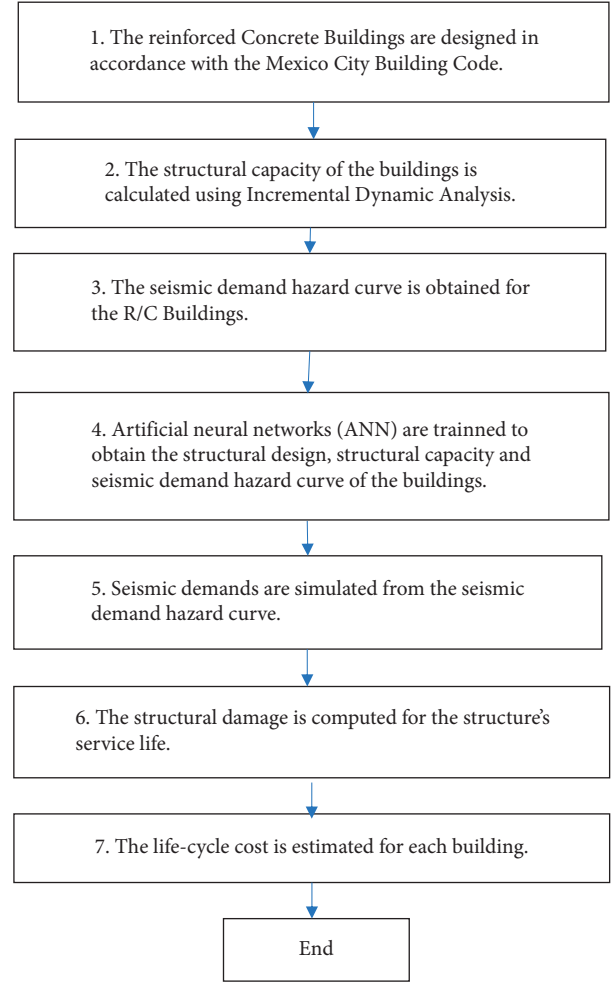


FIGURE 1: Flowchart of the life-cycle cost assessment procedure.

2.3. Structural Reliability (Step 3). The structural reliability is obtained from the seismic demand hazard curve that estimates the mean of the annual rate of exceeding a certain MID. The curve is calculated by the following expression [33,34]:

$$\left| \frac{d\nu(S_a)}{d(S_a)} \right| P(D > d | S_a) d(S_a), \quad (1)$$

Where $\nu_D(d)$: represents the average number of times per year that MID exceed a given value of d ; d : a given value of MID; D : structural demand, presented by the maximum inter-story drift; S_a : pseudo-acceleration associated with the fundamental period of vibration of the building; $\nu(S_a)$: the seismic hazard curve for the site of interest; and

$$P(D > d | S_a) = 1 - \Phi\left(\frac{\ln(D) - \hat{\mu}_{\ln d}}{\hat{\sigma}_{\ln d}}\right), \quad (2)$$

where $P(D > d | S_a)$: is the fragility curve; Φ : the standard normal cumulative distribution function; $\hat{\mu}_{\ln d}$: the median of the logarithmic value of the seismic demand; $\hat{\sigma}_{\ln d}$: logarithmic standard deviation of the demand.

2.4. Artificial Neural Network Training (Step 4). In this study, the artificial neural network technique has been used for the structural design of the buildings and to estimate the capacity and seismic demand hazard curves. From the previous steps, and in order to obtain the structural capacity and seismic demand hazard curve, numerous nonlinear analyses that are time consuming are required. Therefore, it is possible to reduce the time for the analysis of the building using ANN models. The Matlab [35] software was used in this study to develop the ANNs.

2.5. Seismic Demands Simulation (Step 5). Different values of seismic demands are simulated from the seismic demand hazard curve (equation (1)). For the numerical simulation, the average number of times per year that a seismic event occurs with a magnitude equal or greater than 6 is considered $\nu = 3$. The events are modeled by a Poisson process; therefore, the earthquakes follow an exponential distribution. By using the inverse transformation method [36] different values of MID are simulated for the life-cycle of the buildings.

2.6. Damage Index (Step 6). There are different approaches to estimate the structural damage [37,38]. In the present study, the level of structural degradation is estimated from a measure of physical damage, which is represented as a damage index, DI, expressed as the ratio between the global structural capacity of the building and structural demand. The values taken by the DI are between 0 and 1, when DI equals 0 represents no damage in the structure, and DI equals 1 represents the total damage. The DI is defined by equation (3) [39]:

$$DI = \frac{\delta_D - \delta_y}{\delta_u - \delta_y}, \quad (3)$$

Where δ_D : is the maximum inter-story drift demand, which is obtained from the simulation of the seismic demands of the seismic demand hazard curve (step 5); δ_y : is the maximum inter-story drift associated with serviceability limit state (structure without damage), which is obtained from the statistic value of the limit state considered in the incremental dynamic analyses; δ_u : is the maximum inter-story drift associated with incipient collapse.

2.7. Life Cycle Cost Functions (Step 7). The total cost of a structure with an expected life cycle of 50 years is the combination of the initial cost plus the expected damage cost:

$$C_t = C_I + C_D, \quad (4)$$

Where C_t : represents the total cost of the structure; C_I : is the initial cost; C_D : is the cost associated with the damage.

2.7.1. Initial Cost. The initial cost is calculated using an approximated procedure proposed by De Leon [14]. The cost includes direct cost, indirect costs and the utility paid

to the contractor. The direct cost C_{DI} is estimated from the material cost C_M plus the cost of labor, approximately 40% of C_M , $C_{DI} = 1.4C_M$. The indirect cost due to the nonstructural work the contractor has (i.e.: insurance, training, office expenses, etc.) is estimated to be 20% of C_{DI} , $C_{IN} = 0.2C_{DI}$. The constructor fee is 15% of the summation of the direct cost and indirect cost, $U_M = 0.15(C_{DI} + C_{IN})$. The total initial cost can be estimated as the summation of C_{DI} , C_{IN} and U_M , equation (5);

$$C_I = C_{DI} + C_{IN} + U_M = 1.38C_{DI} = 1.93C_M. \quad (5)$$

Where; C_I : is the initial cost; C_{DI} : is the direct cost; C_{IN} : is the indirect cost; U_M : is the utility.

The unit cost of the construction materials C_M is shown in Table 1. For the cost analyses the average cost of concrete and steel in Mexico City is used.

2.7.2. Damage Cost. The damage costs C_D of the structure during its useful life can be express as the following: repair or reconstruction, C_{PR} ; loss of content, C_{PC} ; economic losses, C_{PI} ; injury, C_{PL} ; and loss of life, C_{PV} . The damage cost can be expressed as Eq. (6);

$$C_d = C_{PR} + C_{PC} + C_{PI} + C_{PL} + C_{PV}. \quad (6)$$

The damage costs are obtained by means of the simulated level of structural damage present in the building. The damage index (Step 6) is used to measure the structural damage simulated.

(1) Repair Cost or Reconstruction. There are several methods to repair buildings damaged by previous earthquakes, depending on factors such as the level of damage, type of structure, configuration, logistics. In this study, it is assumed that the R/C buildings will be repaired using the jacketing technique of structural members, this technique allows the structure to be repaired effectively and return to practically its initial condition before the damage. Based on the repair costs of buildings that were damaged by previous earthquakes a relationship between the repair cost and the damage index was established. The structural damage in some cases is extremely severe such structures can no longer be repaired, and it is necessary to be demolished. De León and Ang [40] considered that for $DI > 0.70$ the R/C structure needs to be demolished. The costs of reconstruction are assumed to be equal to $1.2 C_I$, which includes costs of demolition, cleaning and redesigning the structure. For $DI < 0.70$ the repair cost is a function of the initial cost times the DI to the second power. The repair or reconstruction costs are defined by equation (7) and (8):

$$C_{PR} = (C_I)DI^2, \quad 0 \leq DI < 0.7, \quad (7)$$

$$C_{PR} = 1.2C_I, \quad DI \geq 0.7. \quad (8)$$

The relationship between the normalize repair cost (C_{PR}/C_I) and the damage index is shown in Figure 2.

TABLE 1: Unitary cost of materials.

Material	Cost (\$US Dollar)
Steel	\$1000/ton
Concrete ($f_c = 250 \text{ kg/cm}^2$)	\$130/m ³

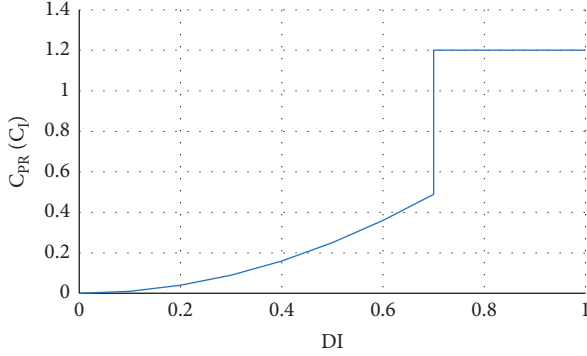


FIGURE 2: Repair cost as function of damage index.

(2) *Cost Due to Damage of Contents.* The estimation of costs due to damage of contents depends on the type and use of the structure; for example, the damage of contents in a school does not have the same impact as that of an office building or shopping mall. In this study, it is assumed that the buildings are offices, it is considered as suggested by Suranhman and Rojiani [41], that the maximum content loss if $DI > 1$ is equal to 50% of the initial cost. For values of $DI < 1$, the expected cost is assumed to be a linear function of DI . The cost due to loss of content is defined by equations (9) and (10):

$$C_{PC} = 0.5(C_I)DI, \quad 0 < DI < 1.0. \quad (9)$$

$$C_{PC} = 0.5C_I, \quad DI \geq 1.0. \quad (10)$$

The relationship between the normalized cost due to damage of contents (C_{PR}/C_I) and the damage index is shown in Figure 3.

(3) *Cost Due to Economic Loss.* The cost due to economic loss depends on the economic activity for which the building is used. This study assumed the usage of the building as offices; therefore, the economic loss is associated with the loss of income due to rental during the time of repair or reconstruction.

The maximum cost for economic loss ($DI > 1$) is a function of the period of reconstruction (P_R), the average rent in dollars per square meter (R) and the build area in meters of the structure (A). For values of $DI < 1$ the variation of cost is assumed to be a function of DI to the second power [14]. The average monthly rental for offices in Mexico City is equal to \$19 US dollars/m² and it is assumed that the maximum period of reconstruction of a building is equal to 24 months. The function due to economic loss is defined by equations (11) and (12).

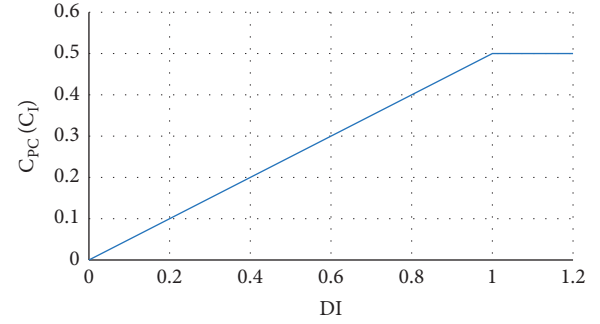


FIGURE 3: Loss of content cost as function of damage index.

$$C_{PI} = R(P_R)A, \quad DI \geq 1. \quad (11)$$

$$C_{PI} = R(P_R)(A)DI^2, \quad 0 < DI < 1.0. \quad (12)$$

The relationship between the normalized economic cost per square meter of building area (C_{PI}/A) and the damage index is shown in Figure 4.

(4) *Cost Due to Loss of Life.* The estimation of the cost associated with life loss is a difficult task because it is a sensitive issue [42–45]. Two postures regarding the value of a person life can be found. The first one, human life has a statistical value based on its income; and the second one, the cost of human life is invaluable. For this work, the value of a life is considered by the average income of a person.

For the present study, the cost due to the loss of life is estimated relying on previous catastrophic seismic events. For this reason, it is necessary to estimate the average number of dead people inside a building during a seismic event. A nonlinear regression analysis [40] was obtained based on the total area of buildings that collapse during the 1985 Mexico City earthquake [46] and the number of deaths [47]. The result of this analysis is summarized in equation (13) and shown in Figure 5:

$$N_d = 45.48 + 5.531744A^2. \quad (13)$$

Where N_D : is the number of deaths; A : is the of collapsed buildings area in 1000 m².

The cost due to the loss of life function ($DI > 1$) is expressed as the total number of deaths, N_D , in the case of incipient collapse, multiplied by the value of the statistical life-time income of a person, C_{PF} . For smaller vales of DI , it is assumed that the cost function can be represented by the total number of deaths, multiplied by the statistical life-time income of a person multiplied by DI to the fourth power, Equation (15). It is considered that the average annual income of a person in Mexico is considered equal to \$10000 US dollars [48], and that the useful working life per person is equal to 25 years, so the cost per death (C_{PF}) of a person is equal to \$250,000 US dollars. The cost functions due to loss of life are summarized in equations (14) and (15) [14]:

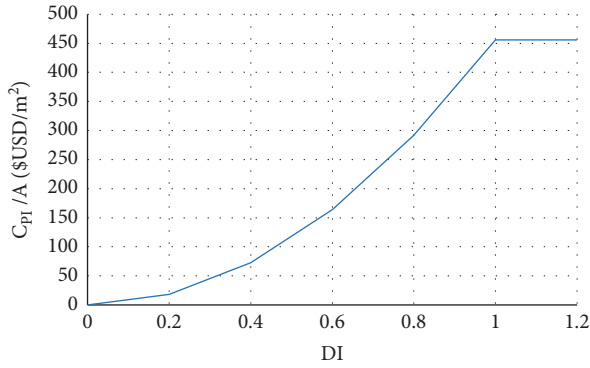


FIGURE 4: Economic loss as function of the damage index.

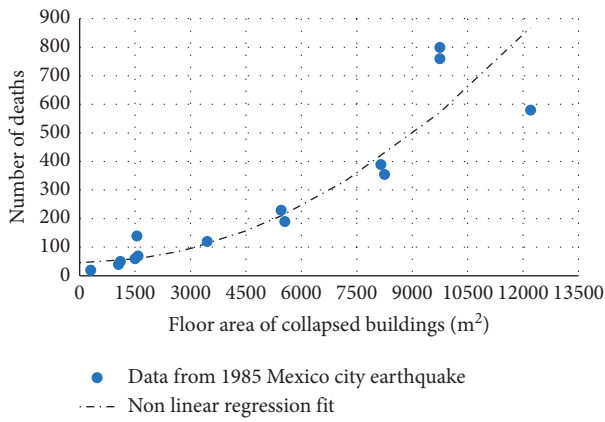


FIGURE 5: Number of deaths vs area of collapsed buildings.

$$C_{PV} = N_D (C_{PF} DI^4), \quad 0 < DI < 1. \quad (14)$$

$$C_{PV} = N_D C_{PF}, \quad DI \geq 1. \quad (15)$$

(5) *Cost Due to Injuries.* The evaluation of cost due to injuries, C_{PL} , refers to expenses required for hospitalization of people who became injured during an earthquake [14]. The average number of people injured per unit area of collapse is equal to $0.0168/\text{m}^2$ estimated as the relation of the number of injuries reported in the 1985 Mexico City earthquake [47] with the total area of buildings collapsed [46]. The cost of injuries without disability, C_{LS} , is considered equal to \$2000 US dollars. Notice that costs for minor injuries, medical expenses and medicine, including a small stay in the hospital are considered. Injured without disability are considered to represent 90% of all injured people [40]. The cost of injuries resulting in disability, C_{LI} , is considered equal to \$250,000 US dollars (equal to the cost of death). People with disabilities represent 10% of total injuries.

For $DI < 1$ the cost due to injuries is assumed to be a function of the total people injured in the building times the DI raised to the second power, Equation (16) [14]. For $DI > 1$ the cost function is assumed to be a function of the total people injured in the building with disability and without disability in the building, Equation (17).

$$C_{PL} = (0.1C_{LI} + 0.9C_{LS})0.0168(A)DI^2, \quad 0 < DI < 1, \quad (16)$$

$$C_{PL} = (0.1C_{LI} + 0.9C_{LS})0.0168A, \quad DI \geq 1. \quad (17)$$

The relationship between the normalized cost due to injuries per person injured (C_{PL}) and the damage index is shown in Figure 6.

3. Illustrative Example

The illustration of the methodology is presented by an example in this section. The methodology is applied to a 12-story, 3-bays reinforced concrete building.

3.1. Selected Ground Motion Records. In this study three different buildings are located in soft soil with a dominant period $T_S = 2.0\text{s}$. A set of 15 ground motion records were selected to perform the analyses of the buildings. Table 2 shows the main characteristics of the earthquake ground motions. The ground motion records were obtained from the IINGEN database [49]. The pseudo-acceleration elastic seismic response spectra of the records selected are shown in Figure 7 considering 5% of critical damping.

Figure 8 shows the seismic hazard curves associated with different fundamental structural periods. Those curves represent the probability that a structure will exceed a specified seismic intensity (e.g., pseudo-acceleration) in one year. The curves are used to solve Eq. 1, and corresponds to a site located at soft soil of Mexico City.

3.2. Reinforced Concrete Building Characteristics. Three types of reinforced concrete buildings, low, mid, and high rise were selected for the seismic analyses and design according with common practice in Mexico City. The buildings were represented by three-dimensional structural models with elevation between 4, 8, and 12 stories, an inter-story height equal to 4 meters. The buildings are constituted by orthogonal rigid reinforced concrete frames constituted by beams and columns, with three bays in both directions. While for the 4-story building the bay length is equal to 6m, for the 8 and 12-story buildings the bay length is equal to 8m. The frames are connected by floor slabs assumed to be rigid diaphragms. Figure 9 shows the geometric characteristics of the buildings.

3.3. Structural Design. The 12-story building is designed in accordance with the Mexico City Building Code [50]. The loads considered for the analysis are; dead load, live load and seismic load.

The 12-story building was divided into 3 groups of beams and 3 groups of columns to uniform the buildings sections. Table 3 shows the results of the structural design for the 12-story building. The sections characteristics shown in Table 3 are the parameters for beams; b: width, h: depth, A_{se} : longitudinal reinforcement inferior at the end region of beam, A_{se}' : longitudinal reinforcement superior at the end region of beam, A_{sm} : longitudinal reinforcement inferior at

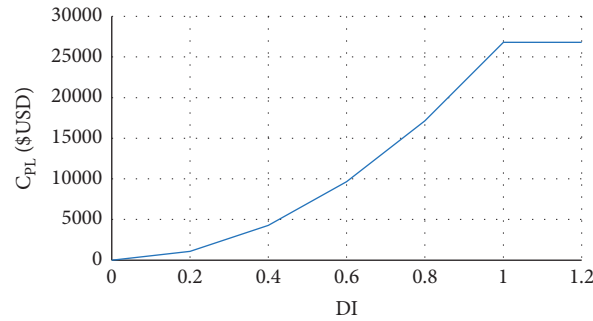


FIGURE 6: Cost of Injuries per person as a function of the damage index.

TABLE 2: Earthquake ground motions recorded on soft soil $T_s = 2.0s$ in Mexico City.

EQ.	Date	Epicenter Coordinates	Magnitude	Station	Location
S1	97-01-11	18.220 N; 102.76 W	6.9	RIDA	RED INTERUNIVERSITARIA DE INSTRUMENTACION SISIMICA (RIIS)
S2	89-04-25	16.603 N; 99.400 W	6.9	DR16	CENTRO DE INSTRUMENTACION Y REGISTRO SISMICO (CIRES)
S3	97-01-11	17.9 N; 103.0 W	6.9	DR16	CENTRO DE INSTRUMENTACION Y REGISTRO SISMICO (CIRES)
S4	95-09-14	16.31 N; 98.88 W	7.3	IMPS	CENTRO NACIONAL DE PREVENCION DE DESASTRES (CENAPRED)
S5	97-01-11	18.09 N; 102.86 W	6.9	IMPS	CENTRO NACIONAL DE PREVENCION DE DESASTRES (CENAPRED)
S6	95-09-14	18.02 N; 101.56 W	7.3	CHAS	CENTRO NACIONAL DE PREVENCION DE DESASTRES (CENAPRED)
S7	89-04-25	16.603 N; 99.400 W	6.9	EO30	CENTRO DE INSTRUMENTACION Y REGISTRO SISMICO (CIRES)
S8	89-04-25	16.603 N; 99.400 W	6.9	CO47	CENTRO DE INSTRUMENTACION Y REGISTRO SISMICO (CIRES)
S9	95-09-14	16.31 N; 98.88 W	7.3	CO47	CENTRO DE INSTRUMENTACION Y REGISTRO SISMICO (CIRES)
S10	81-10-25	17.880 N; 102.150 W	7.3	SXVI	INSTITUTO DE INGENIERÍA. UNAM
S11	85-09-19	18.081 N; 102.942 W	8.1	SXVI	INSTITUTO DE INGENIERÍA. UNAM
S12	95-09-14	16.31 N; 98.88 W	7.3	COYS	CENTRO NACIONAL DE PREVENCION DE DESASTRES (CENAPRED)
S13	95-09-14	16.31 N; 98.88 W	7.3	PII6	CENTRO DE INSTRUMENTACION Y REGISTRO SISMICO (CIRES)
S14	95-09-14	16.31 N; 98.88 W	7.3	FJ74	CENTRO DE INSTRUMENTACION Y REGISTRO SISMICO (CIRES)
S15	95-09-14	16.31 N; 98.88 W	7.3	CS78	CENTRO DE INSTRUMENTACION Y REGISTRO SISMICO (CIRES)

the mid span, As_m : longitudinal reinforcement superior at the mid span, s_e : stirrups spacing at the end of the beam, s_m : stirrups spacing in the middle of the beam, for columns; b : width, h : depth, A_s : longitudinal reinforcement, s : stirrups spacing.

3.4. Building Structural Capacity. The structural capacity of the building is calculated using incremental dynamic analysis. For this aim, the software Ruaumoko3D [51] was used to apply a series of nonlinear structural analyses to the building in order to determine the structural behavior.

Nonlinear structural analysis is performed by subjecting the structure to a set of records (Table 2) scaled at different increasing levels of pseudo-acceleration. The result extracted from each analysis is a discrete point used to form the IDA curve (see Figure 10). The modified Takeda hysteretic model was considered in the analyses to assume the degradation of stiffness and strength of the reinforced concrete elements.

The limit state near collapse is defined within the Ruaumoko computer program when one of the following conditions are reached: (a) Numerical instability, (b) decrement of the tangent lateral stiffness to 20% of the initial value or, c) ultimate rotation condition of a member. The

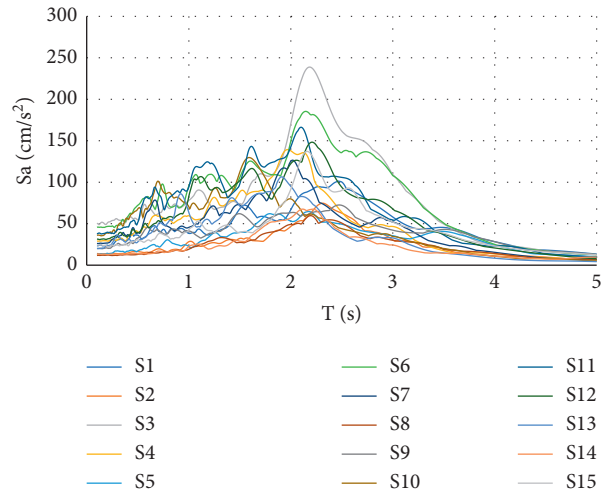


FIGURE 7: Seismic response spectra of the selected ground motions for soft soil with $T_s = 2.0$.

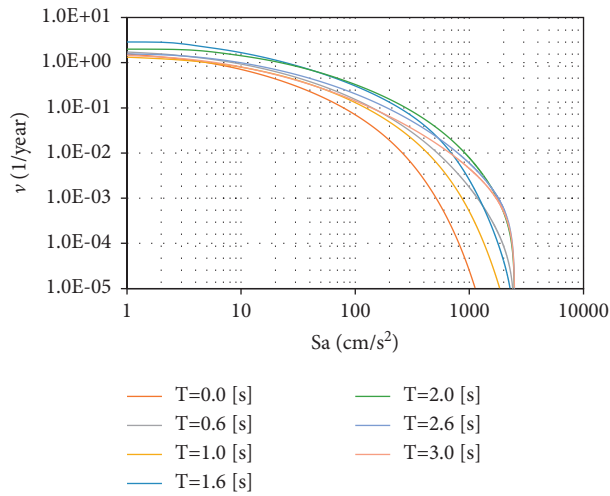


FIGURE 8: Seismic hazard curves.

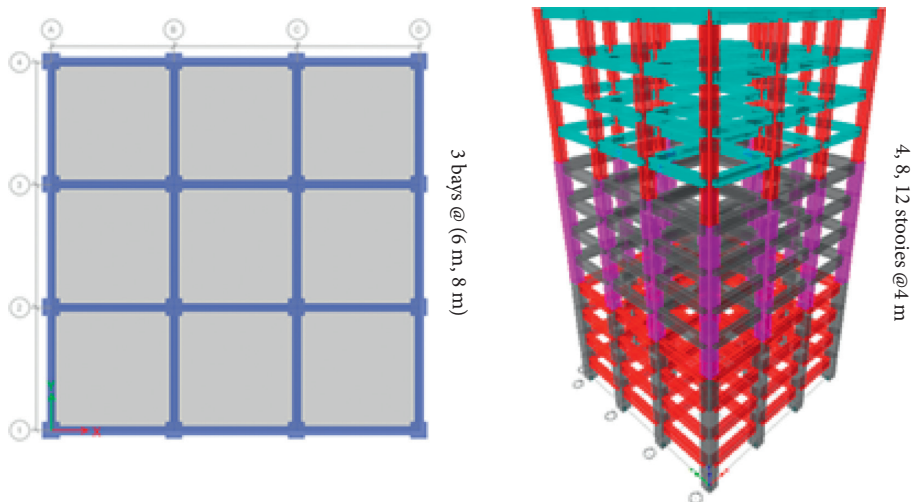


FIGURE 9: Plan and elevation of the reinforced concrete buildings.

TABLE 3: 12-story building structural design.

Parameter	Units	Parameter	Units		
b	70	cm	Ase	41.10	cm ²
h	150	cm	Ase'	29.57	cm ²
Ase	72.21	cm ²	Asm	11.19	cm ²
Ase'	59.77	cm ²	Asm'	15.43	cm ²
Asm	26.66	cm ²	se	6	cm
Asm'	27.46	cm ²	sm	7	cm
se	4	cm	b	130	cm
sm	4	cm	h	130	cm
b	65	cm	As	471.78	cm ²
h	130	cm	s	3	cm
Ase	63.99	cm ²	b	130	cm
Ase'	53.58	cm ²	h	130	cm
Asm	21.32	cm ²	As	286.55	cm ²
Asm'	24.56	cm ²	s	3	cm
se	4	cm	b	110	cm
sm	4	cm	h	110	cm
b	45	cm	As	234.83	cm ²
h	100	cm	s	5	cm

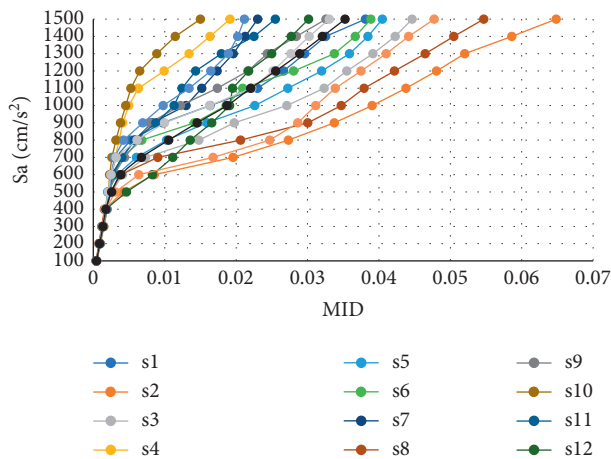


FIGURE 10: IDA curves for 12-story building.

yielding limit state was defined as the difference of 10% of the elastic slope.

3.5. Seismic Demand Hazard Curve. In order to obtain the seismic demand hazard curves, the fragility curves for the 12-story building are needed. The fragility curves represent the conditional probability of damage being exceeded a particular damage state, these curves are obtained from Eq. 2.

Figure 11 presents a set of 12 fragility curves. Those curves show the vulnerability of the building underground motions, it represents the conditional probability of exceeding a maximum inter-story drift (d) as stated in the Mexico City Building Code [50]. Two limit states are considered, the service limit state and near collapse state. This figure illustrates that when a ground motion intensity $S_a = 900 \text{ cm/s}^2$, the probability of reaching or exceeding $d = 0.015$ is approximately 30% for the 12-story building.

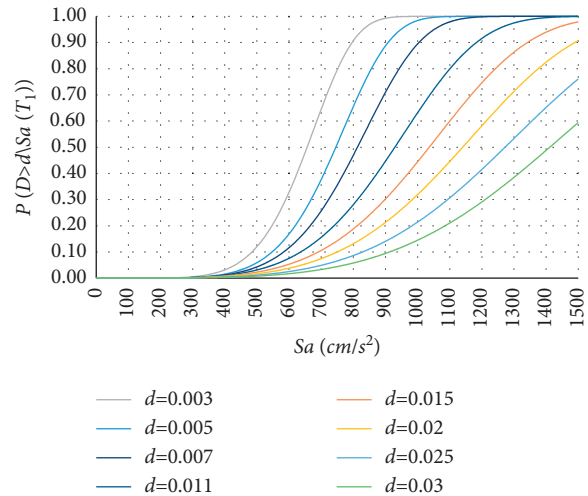


FIGURE 11: Fragility curves for the 12-story building.

From the figure it can be seen that for the same intensity S_a , the exceedance probability (P) decreases as the peak inter-story drift (d) value increases. The seismic demand hazard curve show in Figure 12 was obtained from Eq. 1, and it represents the mean annual rate of exceeding a maximum inter-story drift (d).

3.6. Reliability Analysis Using Artificial Neural Networks. In this study, the technique of artificial neural networks is used, first; to design buildings based on similar characteristics of the buildings used in the database, second; to estimate the structural capacity and the seismic demand hazard curve. Two different ANN models were trained using data from a set of buildings designed in previous studies [52–54].

For the training phase of the first model a feedforward backpropagation network was used to design a 12-story building. The architectural model of the ANN used was an input layer, hidden layers and the output layer, with 7 neurons for the input layer, 5 neurons for the hidden layer and 36 neurons for the output. The activation functions were hyperbolic tangent sigmoid (tansig) for the hidden and output layer. A set of 200 buildings were used as data for the training phase of the first ANN model. The 7 neurons in the input layer represents the general characteristics of the buildings; number of bays in X direction, number of bays in Y direction, story levels, story height, bays spacing X , bays spacing Y , soil period. The 36 output neurons represent the parameters of the beams and columns designed.

The results of the design obtained from the first ANN model are shown in Table 4, which are compared with the results obtained using traditional approaches for seismic design (see Table 3). The results showed excellent similarity with the actual values, attaining a good accuracy prediction with a relative error less than 9%. Moreover, the selected 12-story building was not used in the dataset of the training phase.

The second ANN model estimates the seismic demand hazard curve and capacity of the 12-story building. The input

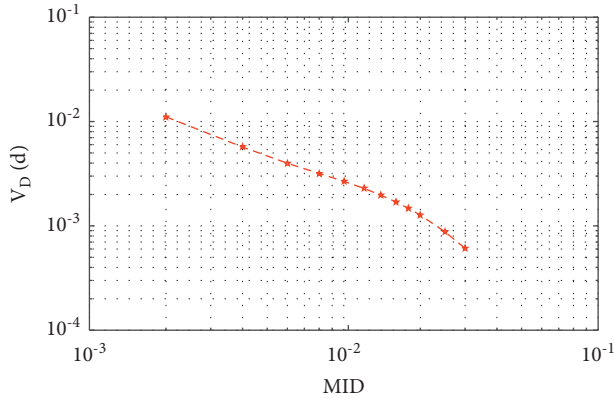


FIGURE 12: Seismic demand hazard curve.

TABLE 4: 12-story building structural design using ANN.

Parameter	Units	Parameter	Units		
b	72.90	cm	Ase	38.72	cm ²
h	155.27	cm	Ase'	24.60	cm ²
Ase	70.73	cm ²	Asm	9.79	cm ²
Ase'	58.54	cm ²	Asm'	13.93	cm ²
Asm	27.85	cm ²	se	6.7	Cm
Asm'	28.54	cm ²	sm	9.5	Cm
se	3.7	cm	b	137.37	Cm
sm	3.6	cm	h	137.37	Cm
b	65.31	cm	As	492.75	cm ²
h	138.69	cm	s	2.4	cm
Ase	62.82	cm ²	b	130.62	cm
Ase'	50.92	cm ²	h	130.62	cm
Asm	22.24	cm ²	As	286.10	cm ²
Asm'	23.74	cm ²	s	3.2	cm
se	4.2	cm	b	106.76	cm
sm	4.2	cm	h	106.76	cm
b	43.24	cm	As	283.24	cm ²
h	90.53	cm	s	5.6	cm

layer with 44 neurons, two hidden layers with 5 neurons and the output layer with 14 neurons, constitutes the architectural model used in the second ANN tool. The same set of 200 buildings was used in the training phase. The activation functions were hyperbolic tangent sigmoid (tansig) for the two hidden layers, and output layer. The input layer parameters are the buildings general and section characteristics and the output layer represents the capacity and seismic demand hazard curve. Table 5 summarizes the input vector parameters.

Figure 13 shows the results of the ANN model and the comparison to those obtained using equation (1). From the figure, it can be seen that the estimation of the seismic demand hazard curve simulated with the ANN; SIM curve, attained good accuracy on predicting equation (1), with a mean square error (MSE) of 2.42e-08 about 9% relative error.

3.7. Seismic Demand Simulation. The simulation of the seismic demands considering 50 years of service life is

TABLE 5: Input vector of the second ANN model.

Input parameter	Units	Input parameter	Units
Number of bays X direction		b	cm
Number of bays Y direction		h	cm
STory levels		Ase	cm ²
Bays spacing X		Ase'	cm ²
Bays spacing Y		Asm	cm ²
Dead load design factor		Asm'	cm ²
Live load design factor		se	cm
Seismic load design factor		sm	cm
b	cm	b	cm
h	cm	h	cm
Ase	cm ²	As	cm ²
Ase'	cm ²	s	cm
Asm	cm ²	b	cm
Asm'	cm ²	h	cm
se	cm	As	cm ²
sm	cm	s	cm
b	cm	b	cm
h	cm	h	cm
Ase	cm ²	As	cm ²
Ase'	cm ²	s	cm
Asm	cm ²		
Asm'	cm ²		
se	cm		
sm	cm		

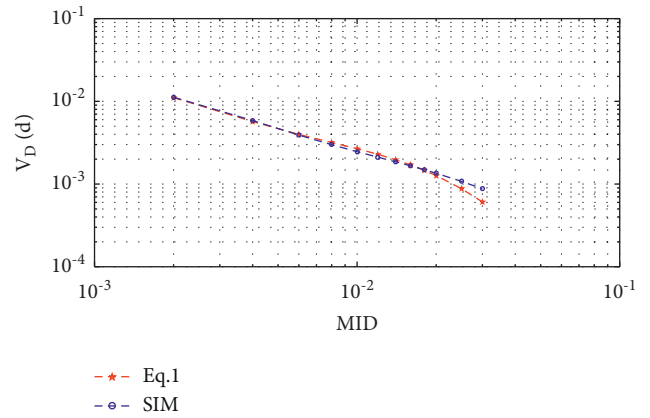


FIGURE 13: 12-story building seismic demand hazard curve results comparison using equation (1) and the ANN model.

performed using the seismic demand hazard curve estimated by the ANN. For the simulation, the average number of seismic events per year is needed, in this study an average number of 3 seismic events with magnitude equal or greater than 6 was used [22]. Figure 14 shows the seismic demands in terms of MID, considering the service life for the 12-story building.

3.8. Damage Index in Service Life of the Building. The damages are evaluated using equation (3). The damage index is then obtained for every seismic demand simulated for the service life of the building. The limit state associated with serviceability, $\delta_y = 0.0018$, and the limit state associated

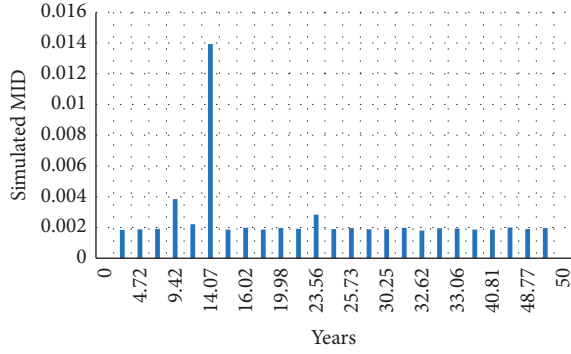


FIGURE 14: Simulated maximum inter-story drift.

with incipient collapse, $\delta_u = 0.0356$, were obtained from the results of the ANN training. Figure 15 shows the damage index for the simulated demands scenario of Figure 14.

3.9. Cost of the 12 Story Building. The initial cost of the 12-story building is obtained from the amount of material (concrete and steel) necessary for its construction. The material is obtained from the quantification of the material necessary to build the beam and column elements obtained from the structural design, 557 tons of reinforced steel and 3660 cubic meters of concrete were quantified. Equation (5) is applied to obtain the initial costs.

$$C_I = 1.93 * ((557 * 1000) + (3660 * 130)) = \quad (18)$$

The damage costs are obtained for the simulated seismic demand of the year 14.07, where the demand is 0.014 for the 12-story building. Applying equation (3) for the year 14.07, the damage index is 0.359 (Figure 15). The costs due to damage are then:

Repair cost or reconstruction (Equation (7)):

$$C_{PR} = (1.993)(0.359)^2 = 0.256 \text{ MM}. \quad (19)$$

Cost due to damage of contents (Equation (9)):

$$C_{PC} = 0.5(1.993)(0.359) = 0.357 \text{ MM}. \quad (20)$$

Cost due to economic loss (Equation (12)):

$$C_{PI} = 19(24)(6912)(0.359)^2 = 0.406 \text{ MM}. \quad (21)$$

Cost due to loss of life (Equations (13) and (14)):

$$N_d = 45.48 + 5.531744(6.912)^2 = 310N_d, \quad (23)$$

$$C_{PV} = 310(250000)(0.359)^4 = \$1.289 \text{ MM}.$$

Cost due to injuries (Equation (16))

$$C_{PL} = (0.1(250000) + 0.9(2000))0.0168(6912)(0.359)^2 = \$0.401 \text{ MM}. \quad (24)$$

The total costs due to damage for the year 14.07 was obtained by the summation of all the costs due to damage (Equation (6)).

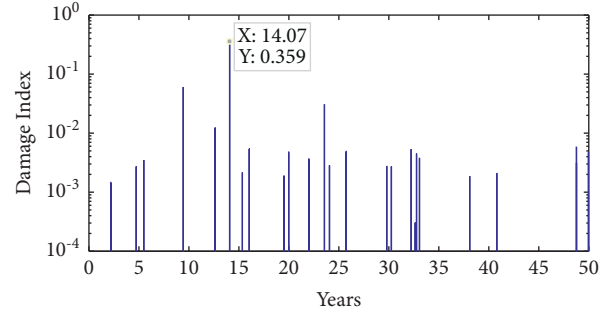


FIGURE 15: Damage index scenario for the service life of the 12-story building.

$$C_d = 0.256 + 0.357 + 0.406 + 1.289 + 0.401 = \$2.709 \text{ MM}. \quad (25)$$

4. Results and Discussion

This section shows the results of applying the methodology for the 4, 8 and 12 story buildings.

The ANN prediction results of the seismic demand hazard curve are compared to those of Equation (1). Figure 16 shows the predicted values of the seismic demand hazard curve for the 4-story building (SIM curve), based on the results of the predictions done by the ANN, the curve shows a deviation from the curve of Eq.1. The mean square error $2.97e-07$ is estimated from the deviation, about a 12% of relative error; therefore, the usefulness of the seismic demand hazard curve to simulate the seismic demand during the life-cycle of the building is sufficient to predict accurate demand values. The seismic demand hazard curve for the 8-story building is shown in Figure 17, where the mean square error estimated from the deviation of the curve predicted by the ANN is $3.81Ee-07$, about a 6% of relative error.

The initial cost of the 4-story building is obtained by applying Equation (5). The amount of material necessary for the construction was obtained from the quantification of the material necessary to build the structural members given by the structural design of the ANN, a total of 39.5 tons of steel and 353.75 cubic meters of concrete were obtained. By applying Equation (5) and multiplying by unit cost of the material (Table 1) the initial cost $C_I =$ US dollars.

Table 6 shows the cost due to damage expected over the life cycle of the 4-story building. From the table it can be seen the damage scenario simulated throughout the 50 year life-cycle of the building, and the damage cost associated with that damage. The total life-cycle cost for the 4-story building is the sum of the initial cost plus the cost due to damage $C_t = 164,991$ US dollars.

To estimate the initial cost for the 8-story building, the ANN was used to design the building and quantify the material necessary for its construction. A total of 230 tons of steel and 1905 cubic meters of concrete were quantified. The initial cost is obtained applying equation (5), the cost is $C_I =$ US dollars. The damage cost for the simulated structural

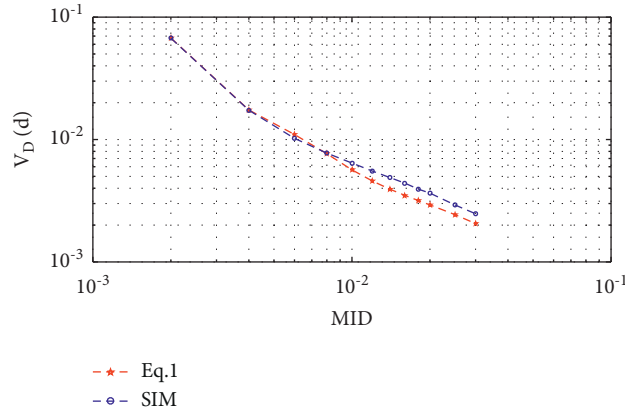


FIGURE 16: 4-story building seismic demand hazard curve results comparison using Equation (1) and ANN model.

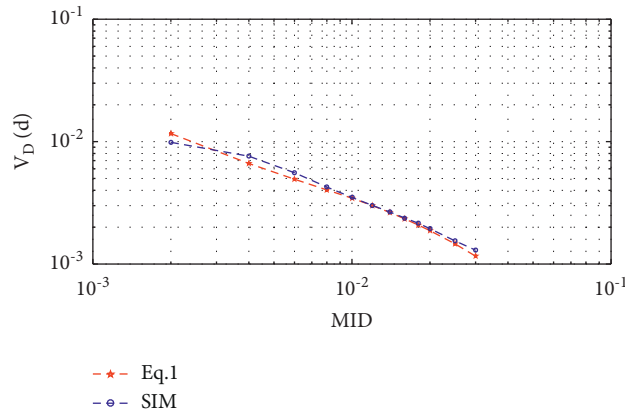


FIGURE 17: 8-story building seismic demand hazard curve results comparison using Equation (1) and ANN model.

TABLE 6: Expected damage cost in the life-cycle of the 4-story building.

Year	DI	C _{PR}	C _{PC}	C _{PI}	C _{PL}	C _{PV}	C _d
0.97	0.0060	\$5.91	\$493.90	\$21.18	\$0.02	\$20.92	\$541.93
1.75	0.1147	\$2,171.08	\$9,463.19	\$7,776.51	\$2,350.17	\$7,678.28	\$29,439.23
5.75	0.0110	\$19.92	\$906.44	\$71.35	\$0.20	\$70.45	\$1,068.35
11.47	0.0365	\$220.10	\$3,013.05	\$788.35	\$24.15	\$778.40	\$4,824.04
17.48	0.0095	\$14.93	\$784.82	\$53.49	\$0.11	\$52.81	\$906.17
31.81	0.0074	\$9.02	\$609.84	\$32.30	\$0.04	\$31.89	\$683.08
37.28	0.0017	\$0.46	\$137.99	\$1.65	\$0.00	\$1.63	\$141.74
39.73	0.0275	\$125.16	\$2,272.15	\$448.32	\$7.81	\$442.65	\$3,296.09
41.52	0.0002	\$0.01	\$14.57	\$0.02	\$0.00	\$0.02	\$14.61
45.87	0.0198	\$64.81	\$1,634.99	\$232.13	\$2.09	\$229.20	\$2,163.23
45.99	0.2157	\$7,677.55	\$17,795.54	\$27,499.99	\$29,389.64	\$27,152.62	\$109,515.34
48.86	0.0420	\$291.58	\$3,468.00	\$1,044.41	\$42.39	\$1,031.21	\$5,877.59
49.86	0.0015	\$0.35	\$120.79	\$1.27	\$0.00	\$1.25	\$123.66
$\Sigma C_d =$							\$158,595

demand scenario of the life-cycle of the 8-story building is shown in Table 7. The life-cycle cost is obtained as sum of the initial cost plus the damage cost, resulting in $C_t = 0$.

The damage cost for the simulated structural demand scenario of the life-cycle of the 12-story building is shown

in Table 8. The life-cycle cost of the 12-story structure is obtained from the sum of the costs associated with damage during the useful life of the structure and the initial cost, for this scenario of simulated demands, the total cost is: $C_t =$.

TABLE 7: Expected damage cost in the life-cycle of the 8-story building.

Year	DI	C _{PR}	C _{PC}	C _{PI}	C _{PL}	C _{PV}	C _d
0.50	0.0031	\$8.6	\$1,408.6	\$19.6	\$0.0	\$19.4	\$1,456.2
0.83	0.0033	\$9.9	\$1,507.5	\$22.5	\$0.0	\$22.2	\$1,562.0
2.64	0.0019	\$3.3	\$868.6	\$7.5	\$0.0	\$7.4	\$886.7
3.44	0.0018	\$2.9	\$822.5	\$6.7	\$0.0	\$6.6	\$838.7
5.21	0.0283	\$738.3	\$13,044.2	\$1,682.8	\$26.0	\$1,661.6	\$17,152.9
17.38	0.0396	\$1,445.6	\$18,252.4	\$3,294.9	\$99.9	\$3,253.3	\$26,346.0
19.84	0.0005	\$0.3	\$246.7	\$0.6	\$0.0	\$0.6	\$248.1
22.98	0.0009	\$0.8	\$422.6	\$1.8	\$0.0	\$1.7	\$426.9
23.66	0.0015	\$2.0	\$680.2	\$4.6	\$0.0	\$4.5	\$691.3
29.72	0.0010	\$1.0	\$480.7	\$2.3	\$0.0	\$2.3	\$486.3
34.72	0.4506	\$187,193.8	\$207,706.1	\$426,679.5	\$1,674,675.4	\$421,289.8	\$2,917,544.6
36.15	0.0004	\$0.1	\$183.3	\$0.3	\$0.0	\$0.3	\$184.1
37.42	0.0025	\$5.9	\$1,171.0	\$13.6	\$0.0	\$13.4	\$1,203.9
38.18	0.0025	\$5.7	\$1,145.5	\$13.0	\$0.0	\$12.8	\$1,177.0
38.39	0.0008	\$0.5	\$352.4	\$1.2	\$0.0	\$1.2	\$355.4
41.94	0.2557	\$60,274.8	\$117,861.4	\$137,387.1	\$173,627.9	\$135,651.7	\$624,802.9
43.56	0.0031	\$8.8	\$1,427.3	\$20.1	\$0.0	\$19.9	\$1,476.2
43.87	0.0002	\$0.0	\$80.0	\$0.1	\$0.0	\$0.1	\$80.1
48.03	0.1104	\$11,231.6	\$50,877.3	\$25,600.7	\$6,028.8	\$25,277.3	\$119,015.6
						$\Sigma C_d =$	\$ 3,715,935
							\$ 3.72 (MM)

TABLE 8: Expected damage cost in the life-cycle of the 12-story building.

Year	DI	C _{PR}	C _{PC}	C _{PI}	C _{PL}	C _{PV}	C _d
2.19	0.0015	\$4.48	\$1,494.98	\$7.09	\$0.00	\$7.00	\$1,513.56
4.72	0.0027	\$14.53	\$2,690.96	\$22.98	\$0.00	\$22.69	\$2,751.16
5.5	0.0035	\$24.42	\$3,488.28	\$38.61	\$0.01	\$38.12	\$3,589.44
9.42	0.0604	\$7,271.89	\$60,197.78	\$11,498.53	\$1,029.06	\$11,353.29	\$91,350.56
12.63	0.0123	\$301.57	\$12,258.82	\$476.85	\$1.77	\$470.82	\$13,509.83
14.07	0.359	\$256,899.01	\$357,798.07	\$406,216.42	\$1,284,313.83	\$401,085.26	\$2,706,312.59
15.35	0.0022	\$9.65	\$2,192.63	\$15.26	\$0.00	\$15.06	\$2,232.60
16.02	0.0054	\$58.12	\$5,381.92	\$91.91	\$0.07	\$90.75	\$5,622.77
19.52	0.0019	\$7.20	\$1,893.64	\$11.38	\$0.00	\$11.23	\$1,923.45
19.98	0.0048	\$45.93	\$4,783.93	\$72.62	\$0.04	\$71.70	\$4,974.22
22	0.0037	\$27.29	\$3,687.61	\$43.15	\$0.01	\$42.60	\$3,800.67
23.56	0.0307	\$1,878.67	\$30,597.22	\$2,970.61	\$68.68	\$2,933.08	\$38,448.26
24.06	0.0028	\$15.63	\$2,790.63	\$24.71	\$0.00	\$24.40	\$2,855.37
25.73	0.0049	\$47.86	\$4,883.59	\$75.68	\$0.04	\$74.72	\$5,081.90
29.8	0.0027	\$14.53	\$2,690.96	\$22.98	\$0.00	\$22.69	\$2,751.16
30.25	0.0027	\$14.53	\$2,690.96	\$22.98	\$0.00	\$22.69	\$2,751.16
32.22	0.0053	\$55.99	\$5,282.26	\$88.54	\$0.06	\$87.42	\$5,514.26
32.62	0.0003	\$0.18	\$299.00	\$0.28	\$0.00	\$0.28	\$299.74
32.77	0.0045	\$40.36	\$4,484.93	\$63.83	\$0.03	\$63.02	\$4,652.17
33.06	0.0038	\$28.78	\$3,787.28	\$45.51	\$0.02	\$44.94	\$3,906.53
38.1	0.0019	\$7.20	\$1,893.64	\$11.38	\$0.00	\$11.23	\$1,923.45
40.81	0.0021	\$8.79	\$2,092.97	\$13.90	\$0.00	\$13.72	\$2,129.39
48.77	0.0058	\$67.05	\$5,780.58	\$106.03	\$0.09	\$104.69	\$6,058.44
48.77	0.0031	\$19.16	\$3,089.62	\$30.29	\$0.01	\$29.91	\$3,168.98
49.97	0.0047	\$44.03	\$4,684.26	\$69.62	\$0.04	\$68.75	\$4,866.70
						$\Sigma C_d =$	\$ 2,921,988.34
							\$ 2.92 (MM)

5. Conclusions

In this paper, a general methodology to obtain the life-cycle costs for buildings located at the soft soil of Mexico City was presented. The costs considered in the analysis are the initial

costs and the cost due to damage. The structural damage was obtained by simulating the damage using the seismic demand hazard curve; however, the number of nonlinear analyses to obtain the curve can be complex and time demanding. This paper proposes a methodology to reduce the

analysis time by using ANNs. The proposed method uses ANNs to model a relationship between the parameters describing the structure and the seismic demand hazard curve. Two feedforward backpropagation network models were selected, the first model was used to obtain the structural design of the buildings, and the second model to obtain the seismic demand hazard curve. The analyzes were conducted considering 3D R/C buildings with varying story height, and bay length subjected to soft soil ground motion records. The performance of the ANN was evaluated by obtaining the seismic demand hazard curve for the different buildings and it was found to be capable of successfully predicting the curves. The accuracy of the developed model was tested by comparing the results of the traditional method and those obtained by the ANNs. The results show that the relative error of the seismic demand hazard curve for the different buildings were between 6% and 12%. It can be considered that the results were acceptable, taking into consideration the computational time reduced from about a few hours when obtaining an exact solution to a few seconds when the ANN model is used. A limitation in the applicability of the presented method is due to the nature of the ANNs that learn the relationships using examples data sets, the particular implementation proposed is then limited to the range of parameters, such as types of buildings, types of soil, properties of materials in construction, etc. Used for the training of the ANNs, any extension of its applicability in other types of buildings will require the generation of additional data to expand the parameters used in the training of the network. Based on the results obtained from the ANN, the seismic demand hazard curves were used to simulate demands in the life-cycle of the structures, from the simulated demands the damage scenario for the life-cycle of the structures was obtained. The total costs of the structures that are given by the initial costs and costs for damage during the useful life were obtained. The total cost obtained in the analysis for the 4-story building was \$323,586 US dollars, for the 8-story building the total cost obtained was \$4.64 million US dollars, and for the 12-story building the total cost during its life-cycle was \$4.91 million US dollars. The proposed approach to obtain the life-cycle cost would be of great use to investors and builders in helping them to consider the future costs of constructing buildings on soft ground in Mexico City. Finally, it is concluded that life-cycle cost is efficiently obtain using artificial neural networks models for the reliability analysis of reinforced concrete building, so it can be used as an excellent planning tool that covers long spans of time.

Data Availability

The data used to support the findings of this study are available from the corresponding authors upon request.

Conflicts of Interest

The authors declare that there is no conflict of interest regarding the publication of this paper.

Acknowledgments

The first author would like to thank CONACYT (Consejo Nacional de Ciencia y Tecnología from México), for the scholarship provided to pursue his PhD studies. The second and sixth author appreciate the support of CONACYT under grant Ciencia Básica 287103. Thanks are given to the PASPA program of DGAPA-UNAM for the support provided to the fourth author. Financial support also was received from the Universidad Autónoma de Sinaloa under grant PROFAPI 2022.

References

- [1] G. Barone and D. M. Frangopol, "Life-cycle maintenance of deteriorating structures by multiobjective optimization involving reliability, risk, availability, hazard and cost," *Structural Safety*, vol. 48, pp. 40–50, 2015.
- [2] P. Castaldo, B. Palazzo, and P. Della Vecchia, "Life-cycle cost and seismic reliability analysis of 3D systems equipped with FPS for different isolation degrees," *Engineering Structures*, vol. 125, pp. 349–363, 2016.
- [3] L. Ierimonti, L. Caracoglia, I. Venanzi, and A. L. Materazzi, "Investigation on life-cycle damage cost of wind-excited tall buildings considering directionality effects," *Journal of Wind Engineering and Industrial Aerodynamics*, vol. 171, pp. 207–218, 2017.
- [4] M. D. Pandey, J. A. M. van der Weide, and J. A. M. Van Der Weide, "Stochastic renewal process models for estimation of damage cost over the life-cycle of a structure," *Structural Safety*, vol. 67, pp. 27–38, 2017.
- [5] U. Vitiello, D. Asprone, M. Di Ludovico, and A. Prota, "Life-cycle cost optimization of the seismic retrofit of existing RC structures," *Bulletin of Earthquake Engineering*, vol. 15, no. 5, pp. 2245–2271, 2017.
- [6] O. Ei-Khoury, A. Shafieezadeh, and E. Fereshtehnejad, "A risk-based life cycle cost strategy for optimal design and evaluation of control methods for nonlinear structures," *Earthquake Engineering & Structural Dynamics*, vol. 47, no. 11, pp. 2297–2314, 2018.
- [7] P. Asadi and I. Hajirasouliha, "A practical methodology for optimum seismic design of RC frames for minimum damage and life-cycle cost," *Engineering Structures*, vol. 202, Article ID 109896, 2020.
- [8] M. Noureldin and J. Kim, "Parameterized seismic life-cycle cost evaluation method for building structures," *Structure and Infrastructure Engineering*, vol. 17, no. 3, pp. 425–439, 2020.
- [9] Y. K. Wen and Y. J. Kang, "Minimum building life-cycle cost design Criteria. I: Methodology," *Journal of Structural Engineering*, vol. 127, no. 3, pp. 330–337, 2001.
- [10] N. D. Lagaros, "Life-cycle cost analysis of design practices for RC framed structures," *Bulletin of Earthquake Engineering*, vol. 5, no. 3, pp. 425–442, 2007.
- [11] C. C. Mitropoulou, N. D. Lagaros, and M. Papadrakakis, "Life-cycle cost assessment of optimally designed reinforced concrete buildings under seismic actions," *Reliability Engineering & System Safety*, vol. 96, no. 10, pp. 1311–1331, 2011.
- [12] L. Esteva, D. Campos, and O. Díaz-L, "Life-cycle optimization in earthquake engineering," *Structure and Infrastructure Engineering*, vol. 7, no. 1-2, pp. 33–49, 2011.
- [13] A. H.-S. Ang, "Life-cycle considerations in risk-informed decisions for design of civil infrastructures," *Structure and Infrastructure Engineering*, vol. 7, no. 1-2, pp. 3–9, 2011.

- [14] D. De León, "Integrating Socio-Economics in the Development of Criteria for Optimal Aseismic Design of R/C Buildings," Ph. D Thesis, University of California, Irvine, EUA, 1996.
- [15] N. D. K. Reddy Chukka, L. Natrayan, and W. D. Mammo, "Seismic fragility and life cycle cost analysis of reinforced concrete structures with a hybrid damper," *Advances in Civil Engineering*, vol. 2021, Article ID 4195161, 17 pages, 2021.
- [16] H. Varae, A. Shishegaran, and M. R. Ghasemi, "The life-cycle cost analysis based on probabilistic optimization using a novel algorithm," *Journal of Building Engineering*, vol. 43, Article ID 1030322021, 2021.
- [17] H. Mirzaeefard, M. Mirtaheri, and M. A. Hariri-Ardebili, "Life-cycle cost analysis of pile-supported wharves under multi-hazard condition: aging and shaking," *Structure And Infrastructure Engineering*, vol. 2021, pp. 1–21, 2021.
- [18] H. Mohammadhassan, B. Behrouz, and R. Maknoon, "A risk-based framework for design of concrete structures against earthquake," *Computers and Concrete, An International Journal*, vol. 25, no. 2, pp. 167–179, 2020.
- [19] S. Shekhar, J. Ghosh, and J. E. Padgett, "Seismic life-cycle cost analysis of ageing highway bridges under chloride exposure conditions: modelling and recommendations," *Structure and Infrastructure Engineering*, vol. 14, no. 7, pp. 941–966, 2018.
- [20] N. Izeboudjen, C. Larbes, and A. Farah, "A new classification approach for neural networks hardware: from standards chips to embedded systems on chip," *Artificial Intelligence Review*, vol. 41, no. 4, pp. 491–534, 2014.
- [21] D. Wang, H. He, and D. Liu, "Intelligent optimal control with critic learning for a nonlinear overhead crane system," *IEEE Transactions on Industrial Informatics*, vol. 14, no. 7, pp. 2932–2940, 2017.
- [22] J. Bojórquez, S. E. Ruiz, B. Ellingwood, A. Reyes-Salazar, and E. Bojórquez, "Reliability-based optimal load factors for seismic design of buildings," *Engineering Structures*, vol. 151, pp. 527–539, 2017.
- [23] Z. Beljkaš, M. Knežević, S. Rutešić, and N. Ivanišević, "Application of artificial intelligence for the estimation of concrete and reinforcement consumption in the construction of integral bridges," *Advances in Civil Engineering*, vol. 2020, Article ID 8645031, 8 pages, 2020.
- [24] H. H. Elmousalami, "Artificial intelligence and parametric construction cost estimate modeling: state-of-the-art review," *Journal of Construction Engineering and Management*, vol. 146, no. 1, Article ID 03119008, 2020.
- [25] T. García-Segura, V. Yepes, and D. M. Frangopol, "Multi-objective design of post-tensioned concrete road bridges using artificial neural networks," *Structural and Multidisciplinary Optimization*, vol. 56, no. 1, pp. 139–150, 2017.
- [26] O. R. De Lautour and P. Omenzetter, "Prediction of seismic-induced structural damage using artificial neural networks," *Engineering Structures*, vol. 31, no. 2, pp. 600–606, 2009.
- [27] P. Alvanitopoulos, I. Andreadis, and A. Elenas, "A New Algorithm for the Classification of Earthquake Damages in structures," in *Proceedings of the 5th IASTED International Conference on Signal Processing, Pattern Recognition and Applications*, pp. 151–156, Innsbruck, Austria, February 2008.
- [28] M. P. González and J. L. Zapico, "Seismic damage identification in buildings using neural networks and modal data," *Computers & Structures*, vol. 86, no. 3-5, pp. 416–426, 2008.
- [29] T. A. Reddy, K. R. Devi, and S. V. Gangashetty, "Multilayer feedforward neural network models for pattern recognition tasks in earthquake engineering," in *Proceedings of the International Conference on Advanced Computing, Networking and Security*, pp. 154–162, Springer, Urathkal, India, December 2011.
- [30] M. A. Orellana, S. E. Ruiz, J. Bojórquez, A. Reyes-Salazar, and E. Bojórquez, "Optimal load factors for earthquake-resistant design of buildings located at different types of soils," *Journal of Building Engineering*, vol. 34, Article ID 102026, 2021.
- [31] J. P. Wang, D. Huang, S.-C. Chang, and Y.-M. Wu, "New evidence and perspective to the Poisson process and earthquake temporal distribution from 55,000 events around Taiwan since 1900," *Natural Hazards Review*, vol. 15, no. 1, pp. 38–47, 2014.
- [32] D. Vamvatsikos and C. A. Cornell, "Incremental dynamic analysis," *Earthquake Engineering & Structural Dynamic*, vol. 31, no. 3, pp. 491–514, 2001.
- [33] L. Esteva, "Bases para la formulación de decisiones de diseño sísmico," PhD thesis, Facultad de Ingeniería, Universidad Nacional Autónoma de México, México, North America, 1968.
- [34] C. A. Cornell, "Engineering seismic risk analysis," *Bulletin of the Seismological Society of America*, vol. 58, no. 5, pp. 1583–1606, 1968.
- [35] Matlab, *Matlab Toolbox, Windows*, The MathWorks, Inc, Natick, Massachusetts, 2015.
- [36] R. Y. Rubinstein, *Simulation and the Monte Carlo Method*, p. 372, John Wiley & Sons, Hoboken Nj, USA, 1981.
- [37] B. Behnam and F. Shojae i, "A Risk Index for Mitigating Earthquake Damage in Urban Structures," *Integrating Disaster Science and Management*, vol. 2018, pp. 3–25, 2018.
- [38] A. D'Ambrisi, M. De Stefano, M. Tanganelli, and S. Viti, "In Book: Seismic Behaviour and Design of Irregular and Complex Civil Structures; Chapter," *The Effect of Common Irregularities on the Seismic Performance of Existing RC Framed Buildings*, Springer, Dordrecht, NY, USA, 2013.
- [39] D. Tolentino and S. E. Ruiz, "Time intervals for maintenance of offshore structures based on multiobjective optimization," *Mathematical Problems in Engineering*, vol. 2013, Article ID 125856, 15 pages, 2013.
- [40] D. De León and A. H. S. Ang, "A Damage Model for Reinforced Concrete Buildings, Futher Study with the 1985 Mexico City Earthquake," in *Structural Safety And Reliability*, G. Schueller et al., Ed., pp. 2081–2087, AA Balkema, Rotterdam, Netherlands, 1995.
- [41] A. Surahman and K. B. Rojiani, "Reliability based optimum design of concrete frames," *Journal of Structural Engineering*, vol. 109, no. 3, pp. 741–757, 1983.
- [42] D. P. Rice and B. S. Cooper, "The economic value of human life," *American Journal of Public Health and the Nations Health*, vol. 57, no. 11, pp. 1954–1966, 1967.
- [43] W. K. Viscusi and E. P. Gentry, "The value of a statistical life for transportation regulations: A test of the benefits transfer methodology," *Journal of Risk and Uncertainty*, vol. 51, no. 1, pp. 53–77, 2015.
- [44] W. K. Viscusi and J. E. Aldy, "The value of a statistical life: a critical review of market estimates throughout the world," *Journal of Risk and Uncertainty*, vol. 27, no. 1, pp. 5–76, 2003.
- [45] T. R. Miller, "Variations between countries in values of statistical life," *Journal of Transport Economics and Policy*, vol. 34, no. 2, pp. 169–188, 2000.
- [46] R. Meli and E. Miranda, *Evaluación de los Efectos de los sismos de septiembre de 1985 en los edificios de la Ciudad de México*, Parte I: Evaluación de daños, Instituto de Ingeniería, México, North America, 1986.

- [47] T. M. Government, "Report in the Investigation of the Earthquake in Mexico," 1985, <https://www.nist.gov/el/earthquake-mexico-1985>.
- [48] Inegi, "Encuesta nacional de ingresos y gastos de los hogares," 2020, <https://www.inegi.org.mx/programas/enigh/nc/2020/>.
- [49] Iingen, "Red Acelerográfica del Instituto de Ingeniería (RAII-UNAM)," Instituto de ingeniería, Universidad Nacional Autónoma de México, 2020, <http://aplicaciones.iingen.unam.mx/AcelerogramasRSM/>.
- [50] Reglamento de construcción del Distrito Federal, *Administración Pública de la Ciudad de México*, Gaceta Oficial de la Ciudad de México, Jefatura de Gobierno, Ciudad de México, México, North America, 2021.
- [51] A. J. Carr, *User Manual for the 3-dimensional Version, ruaumoko3D*, Department of Civil Engineering, University of Canterbury, Christchurch, New Zealand, 2007.
- [52] H. Reyes, *Análisis de sensibilidad de factores de carga, muerta, viva y sismos en edificios desplantados en diferentes tipos de suelo*, Universidad Autónoma de Sinaloa, MC. Thesis, 2019.
- [53] J. Bojórquez, "Combinación óptima para diseño sísmico de edificios," Ph.D. Thesis in Spanish, Universidad Nacional Autónoma de México, Culiacán, Mexico, 2016.
- [54] J. Bojórquez, D. Tolentino, J. Yunes, and S. E. Ruiz, *Diseño de edificios de concreto reforzado utilizando redes neuronales artificiales*, XIX Congreso Nacional de Ingeniería Estructural Puerto Vallarta, Puerto Vallarta, Mexico, in Spanish, 2014.

Research Article

Neural Network Based Estimation of Service Life of Different Metal Culverts in Arkansas

Zahid Hossain ¹, MdAriful Hasan ², and Rouzbeh Ghabchi ³

¹Civil Engineering, Arkansas State University, P.O. Box 1740, Engineering LSW 246, Jonesboro, AR 72467, USA

²Arkansas State University, P.O. Box 1740, Engineering LSW 246, Jonesboro, AR 72467, USA

³Civil Engineering, South Dakota State University, Crothers Engineering Hall 132, Box 2219, Brookings, SD 57007, USA

Correspondence should be addressed to Zahid Hossain; mhossain@astate.edu

Received 31 October 2021; Accepted 9 December 2021; Published 4 January 2022

Academic Editor: Juan Bojórquez

Copyright © 2022 Zahid Hossain et al. This is an open access article distributed under the Creative Commons Attribution License, which permits unrestricted use, distribution, and reproduction in any medium, provided the original work is properly cited.

The Arkansas Department of Transportation (ARDOT) uses different types of metal culverts and cross-drains. Service lives of these culverts are largely influenced by the corrosion of the metals used in these culverts. Corrosion of metallic parts in any soil-water environment is governed by geochemical and electrochemical properties of the soils and waters. Many transportation agencies including ARDOT primarily focus on investigating the physical and mechanical properties of soils rather than their chemical aspects. The main objective of this study is to analyze the geotechnical and geochemical properties of soils in Arkansas to estimate the service lives of different metal pipes in different conditions. Soil resistivity values were predicted after analyzing the United States Department of Agriculture (USDA) soil survey data using neural network (NN) models. The developed NN models were trained and verified by using laboratory test results of soil samples collected from ARDOT, and survey data were obtained from the USDA. The service lives of metal culverts were then estimated based on the predicted soil properties and water quality parameters extracted from the data acquired from the Arkansas Department of Environmental Quality (ADEQ). Finally, Geographic Information System-based corrosion risk maps of three different types of metal pipes were developed based on their estimated service lives. The developed maps will help ARDOT engineers to assess the corrosion potential of the metal pipes before starting the new construction and repair projects and will allow using proper culvert materials to maximize their life spans.

1. Introduction

Metal culverts or pipes are frequently used in Arkansas for different highway drainage structures and irrigation purposes. These culverts are susceptible to significant corrosion. Arkansas has a history of culvert failures and corrosion of the metal culverts was found to be the major reason behind these failures. The Arkansas Department of Transportation (ARDOT) spends a significant amount of money in replacing and installing different types of culverts for cross-drains every year. In 2018, the ARDOT allocated about US\$3.5M for the installation of new and replacement of existing metal pipe culverts [1]. In the coming years, the ARDOT expects to construct and install more metal culverts. The selection of appropriate metallic materials for these

culverts at different construction sites within the state can save future investment and minimize maintenance costs.

The ARDOT's 2014 *Standard Specifications for Highway Construction* document does not provide enough details about the measures needed to be taken to reduce losses due to corrosion [1]. In Section 601 of the ARDOT's 2014 *Standard Specifications for Highway Construction*, the types of metal culverts that can be used in Arkansas are enlisted. According to the ARDOT specifications, zinc coated (galvanized) corrugated steel pipes, aluminum coated corrugated steel pipes, aluminum-zinc alloy coated corrugated steel pipes, corrugated aluminum pipes, asphalt coated corrugated metal pipes, polymer precoated metallic coated corrugated steel pipe culverts, and smooth lined polymer precoated metallic coated corrugated steel pipes can be used

[1]. The corrosion rates of these pipes depend on the materials used in these pipes and their physiochemical properties, type of coatings, properties of soils around the pipes, the quality of surface water passing through the pipes, quality of groundwater, ambient temperature, and other environmental factors. Highly corrosive surface water, abrasive bed materials, and corrosive groundwater can also influence the corrosion of the culverts. Several studies have been conducted in other states to analyze the service life of metal culverts and to prepare risk maps. However, the ARDOT does not have detailed information about the probable spatial distribution of corrosion rates and the expected service life of different metals. Also, no specific guidelines exist for pipe material selection and their installation and/or replacement schedule in Arkansas.

The National Resource Conservation Services (NRCS) used the Survey Geographic Database (SSURGO) and mapped the uncoated steel corrosion risk potentials as low, moderate, and high based on different indicator variables. The NRCS used drainage class and texture of soils, the total acidity of the soil, soil resistivity at saturation, and conductivity of saturated extract for risk classification. The agency has defined the “low” corrosion risk potential when the soil is well-drained and contains coarse-textured particles in combination with a total acidity less than 8 meq/100 g, a resistivity at saturation of at least 5000 ohms/cm, and conductivity of saturated extract less than 0.3 mmhos cm^{-1} . Similarly, “moderate” corrosion risk potential is defined as when the soil is moderately well-drained, in general, with moderately coarse-textured soils, having a total acidity between 8 and 12 meq/100 g, soil resistivity at saturation between 2000 and 5000 ohms/cm, and soil conductivity of saturated extract between 0.3 and 0.8 mmhos cm^{-1} . Finally, “high” corrosion risk potential is considered mostly for fine-textured soils with varied draining conditions, along with a minimum total acidity of 12 meq/100 g, a resistivity at saturation of fewer than 2000 ohms/cm, and conductivity of saturated extract greater than or equal to 0.8 mmhos cm^{-1} (NRCS 2018, [2], and [3]). In this study, risk categories are divided into five different classes based on soil resistivity and pH criteria, and they are applied for mapping purposes.

Tiwari and Manning [4] have developed metal corrosion risk maps for the southern parts of Louisiana. These researchers categorized corrosion potentials into four different types like “mildly corrosive,” “corrosive,” “highly corrosive,” and “extremely corrosive,” based on the expected average life of metal pipes. These researchers used doubly weighted 25×12 matrix to categorize the risk potentials based on the pH and resistivity of soil. The risk matrix was subdivided based on the studies conducted by the Colorado Department of Transportation and Louisiana Department of Transportation and Development and the SSURGO database was used for extracting soil conductivity and pH data.

The main objective of this study is to develop corrosion maps for Arkansas based on secondary data analysis, laboratory test results, neural network (NN) modeling for predicting soil resistivity, and estimation of service life. Relevant literature and guidelines have been reviewed to analyze the best options of the targeted index parameters

based on the available data sources and specific gaps were assessed and addressed accordingly. In this study, galvanized steel pipes (plain), corrugated aluminum (type II) steel pipes, and corrugated aluminum pipe were considered for service life estimations.

2. Methodology

The American Iron and Steel Institute (AISI), the National Corrugated Steel Pipe Association (NCSPA), California Department of Transportation (CALTRANS), Florida Department of Transportation, and a few other agencies in the United States have estimated the service life of different metal culverts for different locations. These agencies have pointed out that resistivity, pH, chloride, sulfate, moisture content, dissolved gases, and bacterial activities in soil and water can influence the service life of a metal pipe. However, most of the agency-developed methods for estimating the service life of metal pipes are based on soil resistivity, soil pH, water resistivity, and water pH. Again, both the outer and inner sides of metal culverts are vulnerable to corrosion. Corrosion in the outer side of the culverts is mainly governed by the soil or backfill material properties and groundwater quality parameters. On the other hand, the inner side corrosion of the culverts is primarily governed by the drainage water quality parameters and abrasive properties of sediments passing through the culverts [5]. The ARDOT does not have details of the spatial variability of these parameters across the state. As a result, an extensive literature review was carried out to estimate the service life and develop metal corrosion maps. In this process, relevant data sources were identified, and relevant data and soil samples were collected. After the literature review, soil resistivity was found as a missing critical parameter in the ARDOT’s typical soil investigation reports. So, an NN-based prediction model was developed to predict soil resistivity based on soil properties provided in the SSURGO and laboratory test results of collected soil samples. Finally, based on the laboratory analysis of collected soil data and secondary data preprocessing and analysis, service lives of metal culverts in different locations of the state were estimated and mapped. A detailed flowchart of the steps involved in this project is presented in Figure 1.

2.1. Secondary Data Collection and Preprocessing. The ARDOT has a database of geotechnical reports from previous construction projects. However, the ARDOT does not have enough data related to electric resistivity and electric conductivity of soils. The United States Department of Agriculture (USDA) has conducted extensive soil surveys within the United States and has documented all the data in an accessible format. The SSURGO database has extensive extractable data comprised of important soil physical and chemical properties (NRCS 2018 and [2]). It has relevant data in the form of 68 different Microsoft-Access (MS-Access) datasets for all 75 counties in Arkansas. Using *Soil Data Viewer*, an add-ins software, data were extracted as

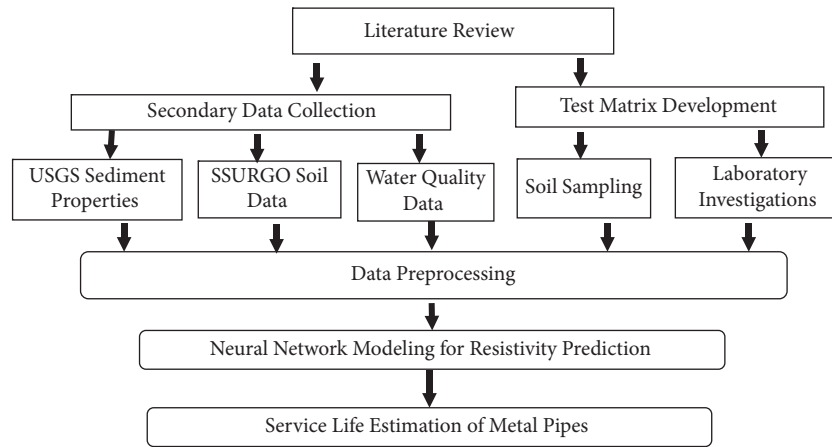


FIGURE 1: Flowchart of the study methodology.

polygon shapefiles of different parishes with corresponding soil properties.

In this study, the Soil Data Viewer tool was added to ArcMap 10.6.1 for the SSURGO data extraction. Feature classes of twenty-one different soil parameters were extracted and merged to create a shapefile related to all the counties in the state. These features were selected based on the factors that are important for corrosion predictions and referred to in different works of literature. The features selected from the SSURGO are as follows: potential risks of corrosion in concrete (categorized as high, moderate, and low), potential risk of corrosion in uncoated steel (categorized as high, moderate, and low), equivalent calcium carbonate content (percent of carbonates, by weight, in the fraction of soil mass which are less than 2 mm in size), cation exchange capacity (CEC-7), effective cation-exchange capacity (ECEC), electric conductivity (EC), gypsum (percent by weight, of hydrated calcium sulfates in the <20 mm fraction of soil), pH, sodium adsorption ratio (SAR), liquid limit, organic matter, percent clay (soil particles that are less than 0.002 millimeter in diameter), percent sand (soil particles that are 0.05 millimeter to 2 millimeters in diameter), percent silt (soil particles that are 0.002 to 0.05 millimeter in diameter), plasticity index, saturated hydraulic conductivity (micrometers per second), AASHTO soil classification, drainage class, depth of water table, flooding frequency class (categorized as none, very rare, rare, occasional, frequent, and very frequent), and ponding frequency class (categorized as none, rare, occasional, and frequent) [2, 6]. After collecting all the soil data from SSURGO, a series of geoprocessing tasks was completed by using ArcMap's toolbox and "ArcPy" module commands to clean and merge them. After merging all the data of all 75 counties, having a total of 334,102 parishes, in Arkansas, all the fields were renamed for keeping the attribute table clean and easily exportable. A summary of the extracted numerical datasets is presented in Table 1. All the data presented in Table 1 are summarized based on the extracted data of the 334,102 parishes that are within the state of Arkansas.

After completion of data extraction, all the polygon layers were dissolved into one layer. The initial geographic

coordinate reference (GCS_North_American_1983) data for all polygons were also converted to the projected coordinate system (NAD_1983_UTM_ZONE_15N). Later on, this projected coordinate system was used for applying all the geospatial interpolations. Geometric features, X and Y coordinates of the center of each polygon, were also added to the attribute table. The final polygon shapefile was named "AR_Dissolved_SSURGO.shp," which had a total of 334,102 polygons. The dataset, "AR_Dissolved_SSURGO.dBase" file, was extracted as a Microsoft Excel spreadsheet. The data were then saved in a different place for further processing and use in the MATLAB programs.

The ADEQ also has an extensive dataset of water quality parameters from different monitoring stations within the state. These datasets are extractable in the Microsoft Excel spreadsheet format. In this study, water pH and total dissolved solid data of the 75 counties were collected and merged with location details. Later the extracted datasets were transformed into point feature layers based on the locations of the stations [7].

2.2. Laboratory Investigations. The SSURGO database has a combination of geotechnical and geochemical parameters of soils. Secondary data collected from the SSURGO have both geotechnical and geochemical data. For gathering additional data and boosting the observation and prediction model development, soil samples were collected from different ongoing construction projects in ARDOT Districts 10 and 02. District engineers were contacted and with their help, 22 soil samples were collected. Geographic locations of the collected soil samples were also collected through ARDOT engineers. Soil resistivity, pH, grain size distribution, Atterberg limits, and specific gravities of the collected soil samples were determined in the laboratory by following ASTM G57, ASTM G51, ASTM D422, ASTM D4318, and ASTM D854 methods, respectively. The description of the soil samples with latitude and longitude of the sampling points, laboratory measurement of soil pH, and resistivity values are summarized in Table 2.

TABLE 1: Summary of SSURGO data of Arkansas.

Field	Min.	Max.	Mean	Standard deviation
CaCO ₃	0.00	14.00	0.06	0.45
Cation exchange capacity (meq/10 g)	0.00	57.50	7.38	10.18
Effective cation exchange capacity (meq/10 g)	0.00	56.70	10.71	8.28
Electric conductivity (mmhos cm ⁻¹)	0.00	8.60	0.20	0.56
Gypsum	0.00	3.00	0.02	0.21
pH	4.30	8.30	5.35	0.65
Sodium absorption ratio	0.00	16.50	0.09	0.78
Liquid limit	4.90	85.00	36.75	11.20
Organic matter content	0.02	4.40	0.66	0.43
Clay (%)	3.50	73.00	28.50	11.67
Sand (%)	1.50	95.00	31.02	19.63
Silt (%)	0.60	77.40	40.45	16.30
Plasticity index	0.00	58.70	16.92	8.80
Hydraulic conductivity (micrometers per second)	0.14	92.00	9.51	12.84
Depth of water table (cm)	0.00	>201	118.18	76.52

TABLE 2: Resistivity and pH testing results of soils.

ID	Description	Latitude	Longitude	pH	R _{min} (ohm-cm)
D10-01	Job no: BR1610	35.830528	-90.764481	6.44	10682.25
D10-02	Monette, AR	35.890578	-90.324728	6.69	11364.82
D10-03	Job no: BB1006	35.984167	-89.875556	6.44	2271.28
D10-04	Job no: 100760	35.611944	-90.203889	7.23	1107.73
D10-05	Job no: 100654	35.903611	-90.291944	6.49	8077.66
D10-06	Job no: 100740	35.888889	-89.911667	6.70	1339.86
D10-07	Job no: 100653	35.903056	-90.237222	6.44	5395.69
D10-08	Job no: 100708	35.997157	-90.562616	7.28	6392.07
D10-09	Job no: 100708	36.056047	-90.621886	7.04	7305.18
D10-10	Job no: 100708	35.830966	-90.512811	6.08	6933.06
D10-11	Job no: 100708	35.830966	-90.512811	7.03	6891.44
D10-12	S Caraway Road, Jonesboro	35.800625	-90.678611	8.33	9187.68
D02-01	Job no: GF 0270	33.654583	-91.211944	7.80	4028.17
D02-02	Job no: 020534	33.134944	-91.855556	6.48	16480.59
D02-03	Job no: 20584	34.100817	-92.001944	5.06	9710.39
D02-04	Job no: BB0203	34.221944	-92.074444	6.49	2168.77
D10-SR01	S Caraway Road, Jonesboro	35.802683	-090.67863	6.40	9234.50
D10-SR02	S Caraway Road, Jonesboro	35.792397	-090.678437	7.26	6770.66
D10-SR03	S Caraway Road, Jonesboro	35.778245	-090.679274	5.66	7608.75
D10-SR04	S Caraway Road, Jonesboro	35.761323	-090.679531	5.91	3448.44
D10-SR05	S Caraway Road, Jonesboro	35.781553	-090.679059	4.78	3569.53
D10-SR06	S Caraway Road, Jonesboro	35.793668	-090.678716	6.21	34554.10

All the data obtained from laboratory investigation were imported to ArcGIS as “soil_sample_data” data. The soil sample dataset had sampling location, sample ID, pH, resistivity, specific gravity, liquid limit, plasticity index, percent sand, percent clay, and percent silt data only. Additional data related to the soil samples were added to the dataset based on the SSURGO data available for the closest geographical location. In the next stage, laboratory investigation data were extracted as a point feature class, “soil_sample_data.” The joined data were finally converted to an Excel-readable format.

2.3. Soil Resistivity Prediction. For developing a soil resistivity prediction model, the exported datasheet (in spreadsheet format) with all dissolved values was further cleaned by removing duplicate rows irrespective of their metadata.

After cleaning 334,102 rows, only 1,927 rows of data were found to be unique and meaningful. However, all of those rows did not have values for EC. Therefore, the dataset was filtered and reduced to rows having EC values. The new dataset having EC values was comprised of 152 rows. Then, the EC values were converted to resistivity values with a conversion factor and the experimental results of 16 soil samples were added to the 152 rows of data obtained from the SSURGO database. Finally, 168 datasets were used to train a shallow neural network fitting tool.

Based on the experience of initial data classification and principal component analysis results, ten parameters were selected for the prediction of soil resistivity. The selected parameters were cation exchange capacity, effective cation exchange capacity, pH, liquid limit, percent organic content, percent clay content, percent sand content, percent silt content, plasticity index, and hydraulic conductivity. After

several trials, the Bayesian regularization-based “trainbr,” a MATLAB function, was selected for developing the neural network models. In the case of selecting several hidden layers and the number of neurons, a simplified approach was used. According to Erzin et al. [8], the maximum number of neurons that can be used for any given number of variables (I) is $2I + 1$. Based on Erzin et al. [8], for ten predictors, a maximum of 21 neurons were considered for training the model. A random process was used for the selection of the datasets for training, validation, and testing at ratios of 75%, 5%, and 20%, respectively. A shallow neural network with having 10 hidden neurons was found to be the best applicable prediction model for the datasets used in this study. A MATLAB function was generated based on the best-performed model, which was finally used to predict the soil resistivity for the rest of the datasets. A summary of performance indicators after training the dataset with different structures of hidden layers is shown in Table 3.

The coefficient of determination (R^2) is a measurement of the performance indicator of any regression model. The training and testing results of the neural network show that one hidden layer with ten neurons has the highest value of R (Table 3). A hidden layer with eight neurons also has comparatively better training and testing performance. From Table 3, it is evident that an increase in the number of neurons resulted in a deterioration in the performance of the model. In the cases of multilayer hidden structures, the model having a two-layer structure with seven neurons in the first layer and three neurons in the second layer was found to exhibit an acceptable performance. However, with an increase in the number of layers and number of neurons, the overall performance was found to reduce. Therefore, based on the performance evaluations, a simple model with one hidden layer of ten neurons was selected as the final model. The R^2 value of the model in the training and overall phases is 0.99 ($R = 0.99$) and 0.57 ($R = 0.75$), respectively. This is a relatively acceptable performance for estimating the soil resistivity of a location lacking any physical resistivity measurements. In other words, the developed NN model can be used to predict soil resistivity by using only the SSURGO data as input parameters.

2.4. Service Life Estimation. The American Iron and Steel Institute (AISI), the National Corrugated Steel Pipe Association (NCSIPA), and many transportation agencies have developed their methods for evaluation of service life of different culverts [5]. For galvanized steel pipes (GSP), the “California Method” is widely accepted and used among practitioners when no prior knowledge of the study site is available. The AISI, the Florida Department of Transportation (FDOT), the Federal Lands Highway (FLH), the Colorado Department of Transportation, the NCSIPA, and the Utah DOT have also developed their methods of evaluating the service life of GSPs. Most of the methods including the “California Method” use resistivity and pH for evaluation of the service life of GSPs. The graphical form of the “California Method” is shown in Figure 2(a) [9], and it has been used for estimating the service life of GSPs in this

study. Aluminized steel (type II) pipe is another common type of culvert used by the ARDOT. The FDOT developed a method based on resistivity, gage thickness, and pH to estimate the service lives of aluminized steel culverts, as presented in Figure 2(b). Aluminum pipe is a material that is commonly used by different state agencies. The FDOT also developed a method to estimate the service life of this type of culvert. A graphical representation of this method is shown in Figure 2(c) [5, 10, 11]. The methods developed by FDOT [10] have been used for the estimation of the service life of aluminized steel and aluminum pipes in this study.

As mentioned earlier, corrosion in the inner side and outer side of the metal pipe is mainly controlled by the water quality parameters and soil or backfill parameters. Part of the pipe connected to the soil bed is more susceptible to corrosion of easier electric passage. For this reason, multiple studies have recommended the use of both the electric resistivity and pH of soil and water for the estimation of service life. In the current study, the electric resistivity and pH of both soil and water were considered, and the minimum estimated service life (in years) was considered as the expected service life of that pipe. To this end, pH values available in the SSURGO database and the soil resistivity predicted from the developed neural network model were used. On the other hand, pH values of water available in the ADEQ dataset were used for estimating the pipe service lives. The resistivity (in ohm-cm) of water was estimated from total dissolved solids (mg/l), available in the ADEQ dataset, by applying a correlation developed by Rusydi [12].

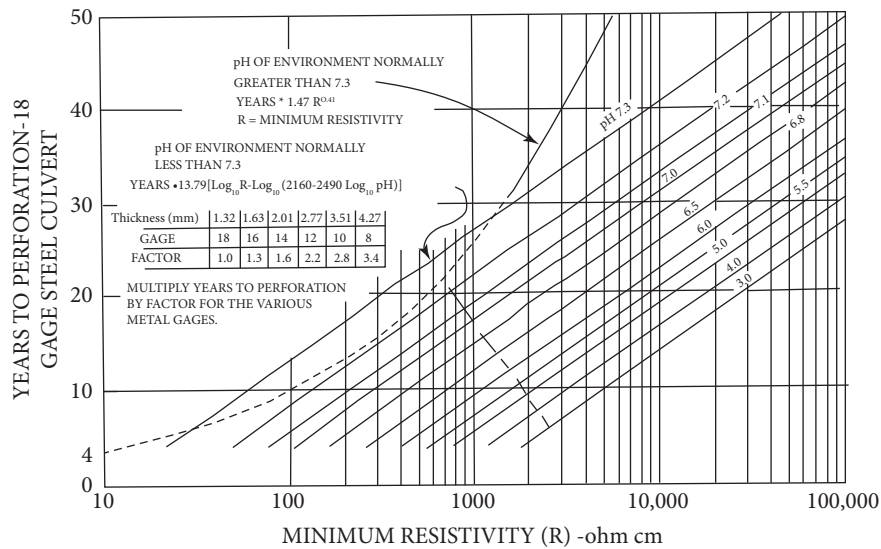
For mapping purposes, the entire state of Arkansas was divided into rasters (size of each raster $250 \text{ m} \times 250 \text{ m}$). Then the nearest neighbor method was applied to assign water resistivity and pH to individual point features. The ArcGIS geoprocessing tool was used for this purpose. Later, the raster features were converted to point features and the Empirical Bayesian Kriging (EBK) technique was applied to develop the interpolated map of predicted service life for different locations in Arkansas. Three different maps were prepared for the three types of selected metal pipes. For comparative analysis, a 16-gage pipe was selected for estimation of the service lives of all three metal pipes. All three methods are based on using resistivity and pH values of the surrounding soil and surface water. Therefore, service lives can be estimated based on the detailed graphs shown in Figure 2. These methods predict the service lives (in years) of the metal pipes, which vary linearly or nonlinearly with the logarithmic scale of resistivity of surrounding media for a particular range of pH. When the pH range varies, the response curves shift. In all three cases, the response curves were found to have positive slopes shifting towards their ordinates with an increase in pH values. Aluminum pipes were found to be less sensitive to resistivity values when compared with the other two types of metal pipes.

3. Research Outcomes

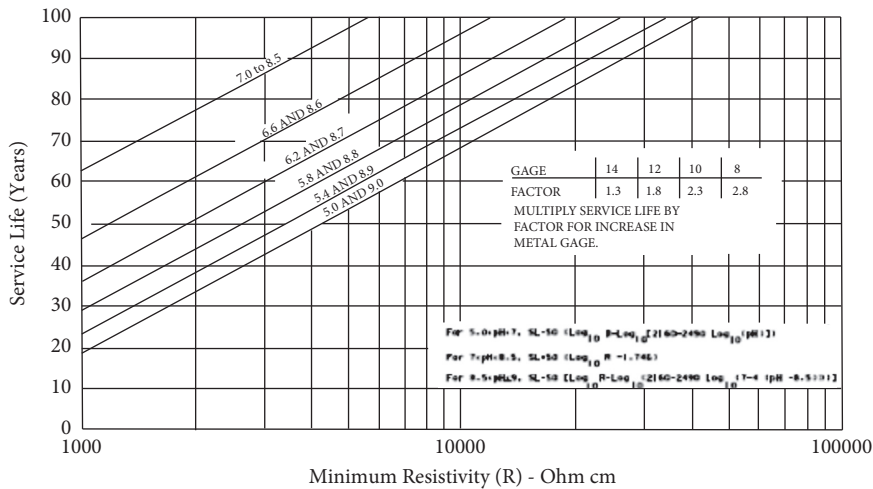
3.1. pH. Based on the data extracted from the SSURGO database, it was observed that the soil pH values varied from 4.3 to 8.3 with an average value of 5.4 and a standard

TABLE 3: Shallow NN training results for prediction of the soil resistivity data after including laboratory test results.

Training function	Trainbr	Trainbr	Trainbr	Trainbr	Trainbr	Trainbr	Trainbr	Trainbr	Trainbr	Trainbr
Hidden layer structure	[10]	[12]	[14]	[16]	[8]	[8 4]	[10 6]	[10 6 2]	[7 3]	[7]
Number of epochs	572	285	1000	331	504	437	683	1000	432	1000
Training—R value	0.99	0.98	0.99	1	0.98	1	0.98	0.99	0.98	0.42
Testing—R value	0.35	0.07	0.06	-0.18	0.20	0.22	0.38	0.14	0.21	0.13
Overall—R value	0.75	0.61	0.59	0.47	0.74	0.51	0.69	0.68	0.74	0.35



(a)



(b)

FIGURE 2: Continued.

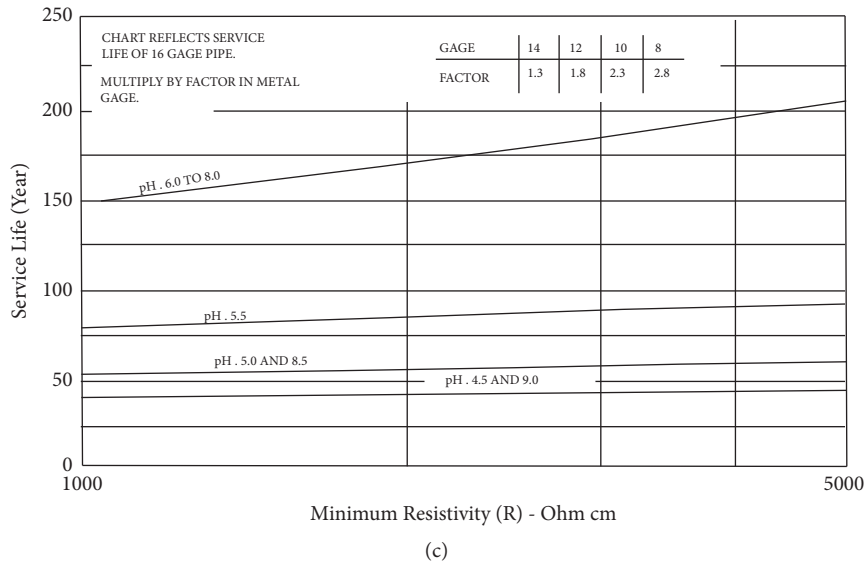


FIGURE 2: Graphical representation of service life estimation methods: (a) 1999 caltrans, (b) 2012 FDOT-aluminized steel, and (c) 2012 FDOT-aluminum.

deviation of 0.65. After dividing all 334,102 Arkansas parishes into 250 m × 250 m raster cells and allocating the same pH within a raster cell, the average pH of 2,137,685 raster cells was found to be 5.51 with a standard deviation of 0.77. The average pH of surface water within the state varies from 1.5 to 10.28, with an average of value 7.0 and a standard deviation of 0.83. The average pH value of soils for each county is presented in Figure 3(a). This map shows that Union, Ouachita, Nevada, Grant, Saline, and Madison counties have pH values of less than 5, which are categorized as “highly acidic.” Four other categories shown in the map are classified as “moderately acidic,” with average pH values between 5 and 5.5, and “acidic,” with pH values ranging from 5.5 to 6.0. For pH ranging from 6.0 to 6.5, the counties are considered as “mild acidic,” and for pH values greater than 6.5, the counties are considered as “not acidic.”

3.2. Resistivity. As noted earlier, one of the main goals of this research is to evaluate the soil resistivity of different locations based on the existing secondary data and collected primary data. Using the secondary data collected from the USDA and laboratory investigation results, a neural network model was developed to predict the soil resistivity of parishes. The predicted average soil resistivity values of each county are plotted in Figure 3(b).

As seen in Figure 4, a few counties (Fulton, Sharp, Izard, Baxter, and Clay) in the northeastern part of Arkansas have low soil resistivity values. In the northwestern part of the state, Newton and Madison counties have very low soil resistivity values. On the western border of the state, three counties (Scott, Howard, and Perry) have very low soil resistivity. In the southern part of the state, two counties (Union and Nevada) have comparatively lower soil resistivity values compared to other counties under study. The rest of the counties in the eastern part have comparatively

higher soil resistivity. Figure 4 shows that the upper basin of the White River has comparatively lower soil resistivity, and the lower basin, a part of the Arkansas River basin, and the Red River basin have comparatively higher soil resistivity. The results obtained based on the model show consistency with the geological map of Arkansas [13]. In general, the average value of soil resistivity of each county varies between 657 and 7698 ohm-cm. For the entire state, the resistivity ranges from 7 to 22515 ohm-cm. The average value of soil resistivity in Arkansas is 3524 ohm-cm with a standard deviation of 4034 ohm-cm. On the other hand, the estimated water resistivity within the state ranges from 264 to 1,62,500 ohm-cm with an average value of 9,156 ohm-cm and a standard deviation of 8,133 ohm-cm.

3.3. Estimated Service Life

3.3.1. Plain Galvanized Steel Pipe (GSP). According to the California method (1993), the service life of plain GSP can be up to 50 years. This method uses resistivity and pH values of the surrounding media (soil and water) as key parameters, and the service life can be estimated based on the technique shown in Figure 2(a). The current study used the previously-determined soil resistivity values and extracted soil pH, water pH, and water resistivity values to estimate the service life GSP at each raster cell for a 16-gage pipe. The service life is estimated separately based on soil pH and resistivity and water pH and resistivity, then the lowest value is reported. For GSP, an estimated service life from 0 to 10 years has been considered as *extremely corrosive*, 10 to 20 years as *highly corrosive*, 20 to 30 years as *moderately corrosive*, 30 to 40 years as *corrosive*, and 40 to 50 years as *mildly corrosive*. Later, the estimated service lives were interpolated over the region. The interpolated GIS raster map for GSP is shown in Figure 4. From Figure 4 it is evident that most of the counties and districts are categorized as extremely corrosive to highly

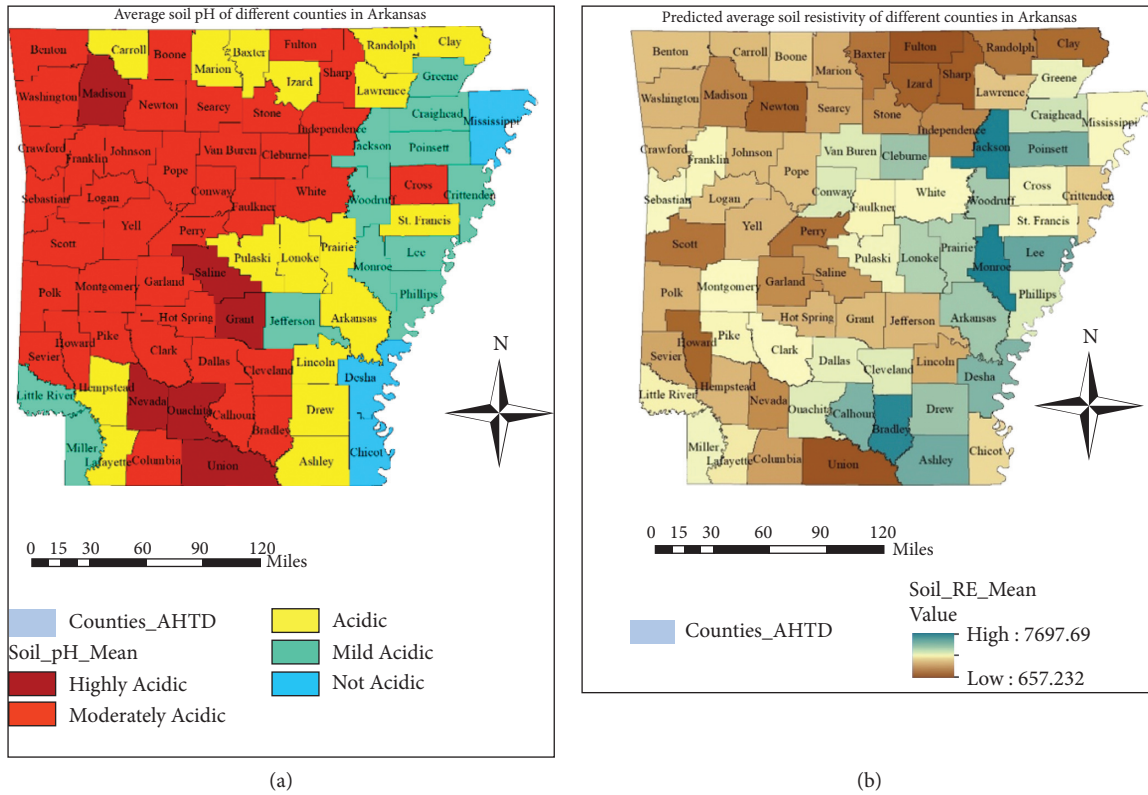


FIGURE 3: Average pH and resistivity of soils in different counties of Arkansas: (a) average soil pH and (b) average soil resistivity.

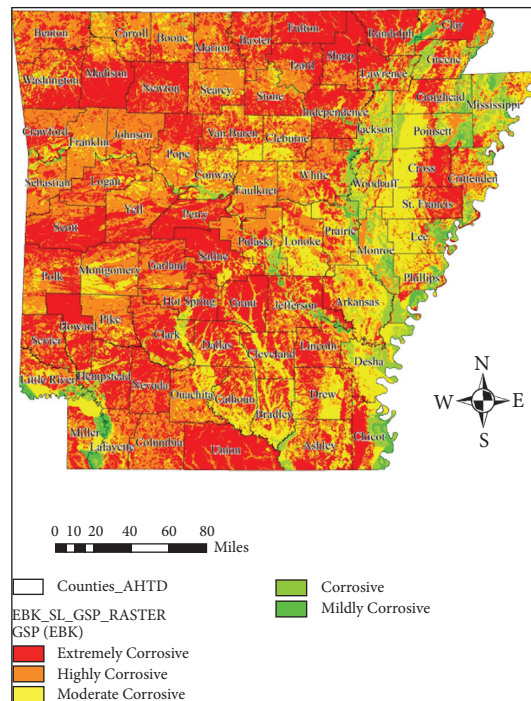


FIGURE 4: Galvanized steel pipe corrosion risk prediction map (generated using EBK).

corrosive for 16-gage GSPs. The service lives for different sizes of GSPs can be estimated by using multiplying factors of 1.6, 2.2, 2.8, and 3.4 for 14-gage, 12-gage, 10-gage, and 8-

gage GSPs, respectively [9]. Based on Figure 4, only the GSPs located in the northeastern part of Arkansas have high expected service lives. In general, most of the parts of the

state should be given careful thought before using any 16 and 18 gages GSPs. Any existing GSPs with 10 years of service or more should be checked as precautionary steps. For future development or construction projects, alternative pipe materials should be taken into consideration for achieving better service lives.

3.3.2. *Aluminized (Type II) Corrugated Steel Pipe.* While determining the service lives of aluminized (type II) corrugated steel pipes, the previously stated approaches of GSPs were used except that for the cases in which the FDOT method instead of the California method was followed. In the interpolated maps developed for this category of pipes, an estimated service life of 0 to 20 years was considered as *extremely corrosive*, 20 to 40 years as *highly corrosive*, 40 to 60 years as *moderately corrosive*, 60 to 80 years as *corrosive*, and more than 80 years as *mildly corrosive*. The interpolated map for aluminized (type II) corrugated steel pipe is shown in Figure 5. From Figure 5, it is evident that a significant portion of the state has moderate to mild corrosion risks, which indicate comparatively higher service lives compared to those of GSPs. However, in some parts of ARDOT Districts 2, 3, 4, 6, 7, and 9, this type of pipe is expected to have a very low service life. Thus, sufficient precautions should be taken to use this type of pipe in these regions. The raster maps shown in Figure 5 are for 16-gage pipes. For different sizes of aluminized (type II) corrugated steel pipes, the service lives can be estimated by using a multiplying factor. These multiplying factors are 1.3, 1.8, 2.3, and 2.8 for 14-gage, 12-gage, 10-gage, and 8-gage pipes, respectively [10].

3.3.3. *Corrugated Aluminum Pipe.* Similar to GSP and aluminized corrugated steel pipes, the service life of corrugated aluminum pipes is estimated based on the FODOT method. For this type of pipe, an estimated service life of 0 to 40 years was considered as *extremely corrosive*, 40 to 60 years as *highly corrosive*, 60 to 80 years as *moderately corrosive*, 80 to 100 years as *corrosive*, and more than 100 years as *mildly corrosive*. Even if the environment is extremely corrosive, this study showed that this type of metal pipe can survive for a very long period. However, the risk of abrasion is very high for this type of metal pipe. So, in the case of selecting this type of metal pipe, the type of sediments that pass through the pipes or culverts should be analyzed before any decisions are made. A detailed interpolated map of predicted service lives of corrugated aluminum type is shown in Figure 6. Figure 6 shows that except for some counties (Union, Logan, Grant, Newton, Lonoke, Independent, Washington, and Crawford), most of the state has soils that are categorized as less corrosive to this type of pipe. Similar to the other two types of pipes, a 16-gage pipe has been considered to evaluate the service life of this type of pipe. For different sizes of corrugated aluminum pipes, the service life can be extrapolated by using a multiplying factor according to the method in [10]. These multiplying factors are 1.3, 1.8, 2.3, and 2.8 for 14-gage, 12-gage, 10-gage, and 8-gage aluminum pipes, respectively.

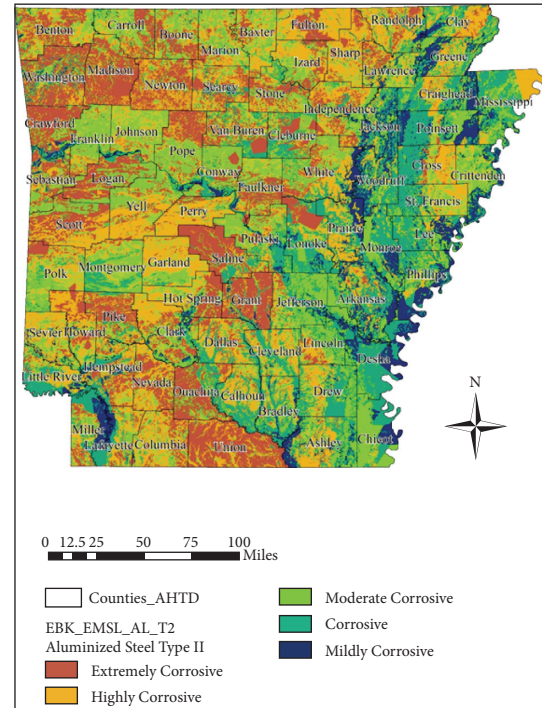


FIGURE 5: Aluminized steel (type II) pipe corrosion risk prediction map (generated using EBK).

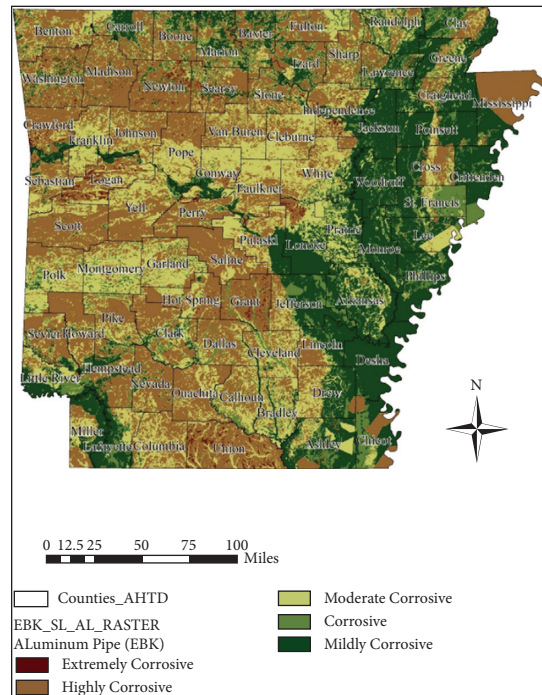


FIGURE 6: Aluminum pipe corrosion risk prediction map (generated using EBK).

4. Conclusions

The main objective of this study was to evaluate the corrosion risk of metal pipes and develop corrosion risk maps for the state of Arkansas. This study has identified the useable secondary data sources and analyzed the available datasets along with

laboratory-based experimental results. Important geotechnical and geochemical properties of soil and water quality data were collected for all 75 counties of Arkansas. Several soil samples were also collected from different locations in the state. Based on the experimental results and collected data from the public domain, a neural network (NN) based model was developed to predict soil resistivity. The water quality data were collected from the ADEQ. Combined soil pH, soil resistivity, surface water pH, water resistivity parameters, and the expected service lives of three types of predominately used metal pipes (plain galvanized steel, aluminized steel, and aluminum) in Arkansas were estimated using the California and FDOT methods. The EBK interpolation method was applied for developing the GIS-based maps that estimate the probable service lives of the three metal types of 16-gage pipes. In general, aluminized corrugated steel pipe or aluminum pipes were found to last longer than galvanized steel pipes. However, the service lives of any of these types of metal pipes varied significantly when they were to be installed in different construction sites within Arkansas. The estimated service lives presented in the maps can be used to extrapolate the service lives of different sizes (gage thicknesses) and other types of metal such as coated pipes.

The findings of this study are implementation-ready and can be immediately used by ARDOT engineers for selecting appropriate metal pipes and maintaining highway drainage pipes. The practice of using these maps will help avoid any unwanted accidents by selecting unsuitable metal pipes in critical areas shown in the maps. Therefore, it is expected to reduce the unnecessary costs associated with the removal and/or replacement of metal culverts. The findings of this study will also help the agency to estimate the condition of the existing culverts installed at critical locations and can be used as a guide for taking the necessary measures to reduce extra expenditure. The developed neural network model can be used for estimating soil resistivity, based on existing secondary data in any location.

One of the limitations of this study is the incorporation of the abrasion levels in the model since they are not easily quantifiable at different locations based on the available sediment data found in the United States Geological Survey database. Therefore, precautions should be taken in selecting aluminum pipes in which abrasion levels play a critical role in determining the service life. The developed neural network model can be updated when new investigation results and additional secondary data are available.

Data Availability

All the data, models, or codes that support the findings of this study are available from the corresponding author upon reasonable request.

Conflicts of Interest

The authors declare that they have no conflicts of interest.

Acknowledgments

The authors would also like to thank District 02 (Mr. Brad Smithe) and District 10 (Mr. Deric Wyatt) engineers for

their effort and assistance in collecting soil samples and providing preliminary data. The technical assistance of Ms. Jami Nash, Mr. Alan Copelin, Dr. Shubhalaxmi Kher, and Dr. Ashraf Elsayed, all from A-State, throughout the project is highly recognized. The authors would also like to thank the other members of the research team at A-State including Mr. Sumon Roy, Ms. Sara Ford, and Ms. Paige Leissner. The authors would like to thank the Transportation Consortium of South-Central States (Tran-SET) for providing funds and technical support to conduct this study.

References

- [1] Arkansas Department of Transportation (Ardot), "Unit price for projects awarded to contract," 2019, https://www.arkansashighways.com/ProgCon/General/bid_tabs_include.aspx.
- [2] U.S. Department of Agriculture (USDA), "National soil survey handbook, title 430-VI," 2018, http://www.nrcs.usda.gov/wps/portal/nrcs/detail/soils/ref/?cid=nrcs142p2_054242.
- [3] M. Hasan and Z. Hossain, "An overview of corrosion risk of metal culverts in Arkansas," in *Proceedings of the 2019 Tran-SET Conference*, San Antonio, TX, USA, April 2019.
- [4] S. Tewari and F. Manning, "Spatial delineation of corrosion zones for metal culverts based on coastal louisiana soil characteristics," in *Proceedings of the Transportation Research Board 97th Annual Meeting*, Washington D.C, USA, January 2018.
- [5] M. Maher, G. Hebel, and A. Fuggle, *Service Life of Culverts—A Synthesis of Highway Practice, Synthesis 474*, National Cooperative Highway Research Program, Washington, D.C, USA, 2015.
- [6] Natural Resources Conservation Service (NRCS), "Web soil survey," 2018, <https://websoilsurvey.nrcs.usda.gov/>.
- [7] Arkansas Department of Environmental Quality (ADEQ), "Water quality monitoring data, laboratory and monitoring services," 2018, https://www.adeq.state.ar.us/techsvs/env_multi_lab/water_quality_station.aspx#Display.
- [8] Y. Erzin, B. H. Rao, A. Patel, S. D. Gumaste, and D. N. Singh, "Artificial neural network models for predicting electrical resistivity of soils from their thermal resistivity," *International Journal of Thermal Sciences*, vol. 49, no. 1, pp. 118–130, 2010.
- [9] Department of Transportation (Caltrans), *Method for Estimating the Service Life of Steel Culverts*, Caltrans, Sacramento, CA, USA, 1999.
- [10] Florida Department of Transportation (Fdot), *Drainage Manual—Optional Pipe Material Handbook. Drainage Section*, Office of Design, FDOT, Tallahassee, FL, USA, 2012.
- [11] American Iron and Steel Institute (AISI), *Handbook of Steel Drainage and Highway Construction Products*, AISI, Washington, D.C, USA, 5th edition, 1994.
- [12] A. F. Rusydi, "Correlation between conductivity and total dissolved solid in various type of water: a review," *IOP Conference Series: Earth and Environmental Science*, vol. 118, no. 1, Article ID 012019, 2018.
- [13] Arkansas Geological Survey (Ags), *Geologic Map of Arkansas, Geologic Maps, AGS*, [https://www.geology.arkansas.gov/docs/pdf/maps-and-data/geologic_maps/geologic-map-of-arkansas-1993-\(34x52\).pdf](https://www.geology.arkansas.gov/docs/pdf/maps-and-data/geologic_maps/geologic-map-of-arkansas-1993-(34x52).pdf), 1993.